공학석사학위논문

Ordering Carbon Nanotubes and Graphene Oxide Via Liquid Crystalline Self-assembly

액정의 자가조립 특성을 이용한 탄소나노튜브와 산화그래핀의 정렬

2014 년 2 월

서울대학교 대학원

융합과학부 나노융합전공

조 혜 란

Abstract

Ordering Carbon Nanotubes and Graphene Oxide Via Liquid Crystalline Self-assembly

HyeRan Jo

Program in Nano science and Technology

The Graduate School

Seoul National University

CNTs and graphene, despite being suitable and attractive materials for future applications such as flexible and transparent devices, have not shown their full potentials in realistic devices for several reasons. CNTs have dispersion problems due to aggregation by van der Waals forces causing the deterioration of performance like, increase of the percolation threshold. In addition, the properties of CNTs are strongly anisotropic and a uniform, controlled alignment is useful for bringing at macroscopic scale the nanoscopic properties, thus enhancing performances in several applications. Like CNTs, graphene flakes, due to their anisotropic shape can benefit from good organization. In this thesis, therefore, I present my research work on self-organized carbon nanomaterials describing two aspects: 1) the dispersion and organization of carbon nanotubes using lyotropic LC systems based on very low concentration of surfactants and 2) organized photoactive composites of graphene oxide.

First, we introduce the concept of Krafft temperature which is the minimum

temperature at which surfactants form micelles. Surfactants are useful for dispersing CNTs but the excess cause deterioration in the properties of CNT and the formation of micelles responsible for the CNT re-aggregates due to depletion attraction The use of the Krafft temperature has been proven advantageous for minimizing surfactants in CNT suspensions while obtaining good dispersions. . So far the process was uncomfortably performed below room temperature. Here new sub-Krafft procedure is presented using OTAB (octadecyltrimethylammonium bromide) surfactant which can be conveniently employed at room temperature. Optical microscopy and spectroscopy, together with atomic force microscopy (AFM), were performed for assessing the quality of the dispersion of CNTs with the surfactants. Dispersions prepared at temperatures above and below the Krafft temperature were analysed and compared finding superior performance for the samples prepared with our novel sub-Krafft approach. Not only aggregates were not distinguishable by optical microscopy but higher average absorption and more intense peaks were measured by optical spectroscopy. The good quality of the dispersion at nanoscale was confirmed by AFM.

Then, lyotropic liquid crystals (LCs) based on surfactants were used as efficient hosts for aligning CNTs. In order to form lyotropic LCs with reduced surfactant content one key idea was the combination of cationic and anionic surfactants. I investigated the effect of changing the ratio of the two surfactants, sodium dodecyl sulphate (SDS) and dodecyltrimethylammonium bromide (12TAB), monitoring the formation of LC phase by Polarized Optical Microscopy. We succeeded in realizing an LC phase with just 8wt%, of surfactants which is an extremely low amount since typically formed lyotropic LC phases are achieved with over 20wt%. The good incorporation of CNTs into the LC host was observed by normal and polarized optical microscopy. The alignment of CNTs in filaments made from the LC-CNT composites was monitored by Polarized Raman spectroscopy.

Graphene oxide, intermediate step in the graphene production by chemical methods, can show nematic LC phase above certain concentrations in water, which means that is a lyotropic LC system. Here, we show the optical characterization of the LC phase of our graphene oxide possessing ultra-large flakes for different GO concentrations. The LC properties of systems combining graphene oxide with chromophores, porphyrin derivative was used here, were also investigated together with the resulting optical properties. Orientational order of graphene with chromophores by LC phase is attractive for applications such as for photovoltaics due to the possibility of optimization of conductive paths. Indeed, the mixtures, GO/porphyrin and rGO/porphyrin, displayed interaction as suggested from the optical spectra and convincing quenching phenomenon from fluorescence spectroscopy.

Keywords(6) : Carbon Nanotubes (CNTs), Liquid Crystal (LCs), Graphene Oxide(GO), Raman spectroscopy, Self-assembly, Nanoparticle composites, Photovoltaics

Student Number : 2012-22453

Contents

List of Figures and Table

images with the same style line of segments. All scale bars indicate 500nm.

Figure 6 Molecular structures of SDS and 12TAB which have the same length of carbon chain and cationic and anionic headgroup respectively.

Figure 7 Lyotropic LCs, between macroscopic crossed polarizers, formed by different ratios of SDS and 12TAB. (A) 2.3 to 1, (B) 2.5 to 1, (C) 2.7 to 1. The overall concentration, for all samples, is equal to 8wt% in DI-W. (B) The sample strongly shows LC phase but the samples (A) and (C) have only shear induced LC phase.

Figure 8 The optical images between crossed polarizers of lyotropic LCs filled into capillaries (0.1mm x 2mm). The mixtures were prepared with different ratios of SDS and 12TAB ; **(**A) 2.3 to 1, **(**B) 2.5 to 1, **(**C) 2.7 to 1

Figure 9 The change of LC phase as temperature increases from 21.6℃ to 42.2℃, observed between crossed polarizers. The ratio between SDS and 12TAB of samples are equal to (1) 2.3: 1, (2)/(4) 2.5 : 1, (3) 2.7 : 1. In case of (4), OTAB solution, which is same solution used in CNT dispersion, is added to the sample with 2.5 ratio.

Figure 10 Polarized optical microscope images of LLC samples with ratios (A) 2.3 to 1, (B) 2.5 to 1, (C) 2.7 to 1, filled into capillaries for measurements of phase transition behavior. (D) The scheme of micelle shape change as effect of temperature change around the phase transition temperature.

Figure 11 (A) Raman spectra of HiPco SWCNT and (B) graphene oxide with 514.5nm laser wavelength.

Scheme 2 The scheme of polarized Raman spectroscopy set-up

Figure 12 LC-CNT mixtures formed with different ratios of SDS and 12TAB, (1) 2.3 to 1 and (2) 2.5 to 1 and (3) 2.7 to 1. They are filled into flat capillaries imposing shear force.

Figure 13 The phase transition temperature between nematic and isotropic phase changed by adding CNTs in samples with ratio 2.7: 1(A, B), 2.6:1(C, D), 2.55:1(E, F). The samples were heated in a hot stage during the optical microscope investigations. The images (A), (C), (E) are of the pure LC phase and (B), (D), (F) for LC samples doped with CNT. The scale bar corresponds to 500μm.

Table 1 The changes of phase transition temperature for each sample before and after adding CNTs

Figure 14 Optical microscope image of (A) same capillary with 2.5 : 1 sample, as in sample 1 of Figure 13 one day after filling, (B) under the polarized optical microscope and (C) 2.5 : 1 sample filled into the capillary a day after the preparation of the LC-CNT mixture,(D) under the polarized optical microscope.\

Figure 15 (A) Easily produced filament from LC-CNT composite for aligning CNTs along the fiber direction. (B) Scheme of the directions of fibers and polarization of incident laser. The upper one (solid line) is the polarization direction of incident laser parallel to the fiber axis and the bottom one (dotted line) is perpendicular. (C) Raman mapping images of G-band using the two perpendicular directions of light polarization. The size of the scanned area is 50μm X 50μm for checking the presence of macroscopically ordered domains. (D) Raman spectra of aligned CNTs measured with two perpendicular directions of light polarization. Two type of lasers were used, 514.5nm and 632.8nm laser wavelengths.

Figure 16 (A) GO suspension (2.5mg/ml) after synthesis and (B) freeze dried sample for the concentration determination.

Figure 25 Fluorescence spectra of (A) porphyrin and GO/porphyrin mixture (the ratio between GO and porphyrin is equal to 250:1) and (B) porphyrin and rGO/porphyrin mixture with 250:1 ratio.

Chapter1 Motivation

Carbon nano-materials are being spotlighted as best candidates to overcome current material limitations. In particular, carbon nanotubes (CNTs) and graphene come to the forefront, attractive for many different electronic applications such as flexible, conductive and transparent layers for displays, solar cells and sensors,[1,2] due to their excellent electrical conductivity, high optical transmission, outstanding mechanical and thermal properties and chemical stability.

CNTs are, however, confronted with many issues that need to be addressed to benefit from their intrinsic, outstanding properties for a proper commercial exploitation and further developments, i.e. the dispersion and the control of the organization of CNTs. [3.4] The problem of aggregation of CNTs, shared with other types of nanoparticles, is due to the strong van der Waals forces between tubes, and seriously downgrades the nanotube performance. For example, CNTs, due to their very high aspect ratio show order of magnitude lower percolation threshold, for the formation of conductive networks, compared to other conducting particles. However, this effect is not manifest when the nanotube dispersion is poor. In addition, due to the high aspect ratio, it is highly desirable to have the nanotubes uniformly aligned into chosen directions, along which properties would then be maximized.[5] In fact, CNTs properties differ along or perpendicular to the tube long axis, thus lack of organization can strongly contribute to failure in the transfer of the pristine properties from the nano to macroscopic scale Different methods for controlling the alignment have been developed and among those an efficient one is the growth of aligned CNT arrays. The problem of this method is the poor control on nanotube properties and purity. A diversity of CNTs exists with potentially different properties and is mixed with impurities and by-products. Because of the great progress in purification and sorting methods [6] of tubes with specific band-gaps, it is desirable to use post-growth organization methods that would allow the

use of any type of desired tubes. We explore the use of liquid crystal hosts for transferring the order from the host to embedded nanoparticles [7]. Liquid crystals are well known for their successful use in display technologies due to their optical properties and their strong response to small electric fields. These amazing and peculiar properties are based on the self-organization ability of liquid crystals. Therefore the self-organization becomes very attractive also for other uses like for manipulating particles at nanoscale at the same reaching macroscopic organization.

As previously mentioned, the dispersion of carbon nanotubes is a big problem. The most common strategy is to disperse CNTs with the aid of surfactants, [8] amphiphilic molecules consisting of hydrophobic and hydrophilic parts. In general, surfactants have headgroups possessing polarity and carbon chain tails. The surface of untreated carbon nanotubes is hydrophobic, which make it impossible to dissolve them into water. When tails of surfactants adsorb on the surface of CNTs , headgroup polarity surrounds CNT helping them to disperse in aqueous solution . The nanotubes tend to aggregate with each other by van der Waals attraction which should be avoided for obtaining good and stable dispersions. Surfactants are also useful for efficiently counteracting the re-aggregation forces but their excess after dispersing CNTs is also detrimental since they spontaneously form micelles by which CNTs re-aggregate due to depletion attraction. [9] Remains of surfactants can also negatively deteriorate device performance thus it is desirable to reduce it. Moreover, only when CNTs are individually dispersed, they display their excellent electrical and mechanical properties. Therefore it is desirable to find a way to reduce the excess of surfactant that degrade the properties of pristine CNTs, at the same time keeping efficient nanotube dispersion.

We introduce the concept of *Krafft temperature* which is the minimum temperature at which the surfactant forms micelles. Below the Krafft temperature (T_k) the excess of surfactant, above the solubility limit, crystallizes and sediments at the

bottom. Based on this property, a method for efficiently dispersing CNTs, leaving minimal residual surfactant, was developed. In previous work[10], we used, as surfactant for dispersing CNTs, CTAB(cetyltrimethylammonium bromide), which is awkward to deal with since had a Krafft temperature below room temperature. Here a procedure is presented to disperse carbon nanotubes using the sub-Krafft method but conveniently adapted to work at room temperature. A surfactant of the same family as CTAB, OTAB (octadecyltrimethyl-ammonium bromide), is chosen due to convenient control at RT. Lyotropic liquid crystals, based on surfactants, are able to host high concentrations of well dispersed CNTs and align them at the same time. [11-15] Since surfactants, as mentioned above, can have adverse effect on the nanotube properties, it is interesting to explore the possibility of an aligning host based on a low amount of surfactant. At this end a very low surfactant LC host was realized for organizing CNTs. The composite was successfully realized obtaining a host composed by almost ¼ of the surfactant used in published works. [15]

Graphene is at the top of the list among materials that can fulfill requirements for the next generation of applications because it has not only excellent material properties as CNT but also additional advantages like two-dimensional flat shape, patternability and so on. It is therefore expected that it will be easier for graphene to overcome the limitations for applications. Among the various ways of producing graphene, the synthesis by chemical methods has considerably great advantages due to the easy and versatile processability and mass production potential, although there are drawbacks like the size and quality of graphene flakes, compared to physical synthesis. Chemical methods, furthermore, can go through the production of graphene oxide (GO) that is water soluble, unlike graphene and, interestingly, the flakes can orient along a preferential direction due to their anisotropic shape.

We want to realize an organized composite based on graphene as light harvesting system for photovoltaics, using graphene flakes and chromophores as photoactive layer. Promising performance has been shown in the literature for such systems. We selected porphyrin as chromophore because they show strong light absorption in the visible. The molecules of chromophore were mixed with GO, obtaining a system that self-assembled into LC phases. The self- organization is expected to impact on charge paths bringing an improvement in the final conductivity

Chapter2 Introduction

2.1 Carbon nanotubes and graphene: structure and properties

The great interest on carbon nanotubes(CNTs) started after the publication of a Nature article by Iijima in 1991.[16] Despite their recent discovery, they are not just man-made material, since they can be found also in natural process and they were even existing 400 years ago as found in an ancient Damascus sabre.[17] Nowadays they are commercially synthesized with a variety of methods like high pressure carbon monoxide(HiPco) process, laser ablation, arc-discharge and especially chemical vapor deposition, for industrial use . They are composed of carbon atoms arranged in a honey-comb lattice and forming a tube as suggested by the name. CNT can be considered as the smallest solid state material since it can stably exist with a tube circumference as small as 10 atoms. Nanotubes have nanometer scale diameters but lengths order of magnitude larger up to millimeters or even centimeters making them an almost 1-dimensional material. Furthermore, outstanding properties are observed in many aspects of material properties: ~1.25TPa(SWNT), 0.27~0.95TPa(MWNT) in Young's modulus, ~200kS/cm in electrical conductivity, ~6600W/mK(SWNT), 3000W/mK(MWNT) in thermal conductivity and so on. CNTs can be metallic or semiconductive, the latter exhibiting different band gaps. [18]

They can be simply described as result of rolling-up one layer of graphite (graphene). When only a single layer graphene is rolled up, it becomes Single-Walled CNT (SWCNT), typically having diameters ranging from 0.4 to 3nm. When several layers are used, Multi-Walled CNT (MWCNT) appears with several concentric carbon walls and diameters up to 200nm. The different ways to roll-up the graphene layer makes CNTs with different properties affecting the band structure, the conductivity and so on. The chiral vector is used to describe the

different orientation of the graphene sheet during the virtual rolling-up process. Different tube structures can be identified such as armchair, zig-zag or chiral which have also different conducting properties.

Graphene is a single layer of graphite, with carbon atoms forming a honey-comb lattice. Graphite is formed by graphene layers stacked on top of each other, interacting only by weak van der waals forces. Graphene can be seen as the thinnest existing film being only one atom thickness (0.34nm). As CNTs, graphene has sp2 hybridization of carbon atom. All atoms are trivalent meaning that three valence electrons participate in bond formation and the forth valence electron is left over. The residual electrons are shared by all atoms in the plane and behavior like free electron. Thanks to their structural specificity, graphene has remarkable intrinsic properties:, 1.1TPa in Young's modulus,[19] mobility of charge carriers (200,000 cm^2/Vs), [20] zero band gap ,~5000 W/mK in thermal conductivity. [21]

2.2 Lyotropic liquid crystal

Liquid crystals are materials possessing fluidity yet a degree of order. Many people, when they think at liquid crystals, they come up with thermotropic liquid crystals because they are widely used in display industry. Lyotropic Liquid Crystals (LLCs), however, were discovered much earlier and are common in everyday life with soap, or cell membrane in our body.

Lyotropic Liquid Crystals are simply formed by self-assembled building blocks of soap molecules (surfactants), in rod- or disk-like micelles, anisometric nanoparticles, DNA and viruses. In lyotropics the concentration is a key parameter, in case of surfactants, determining first the formation of aggregates and then influencing the formation of liquid crystal phases. In other words, micellar shape can be changed from sphere to rod, to layers as the concentration of surfactant molecule increases, and, at same time, achieving organization with orientational

and, eventually some type of lattice order. Spherical micelles organize into the cubic phase at 30~40wt% while cylindrical ones into the hexagonal phase at 40~70wt%. They start to form layered phase at higher concentration around 6~80wt% which has less viscosity than the hexagonal phase since each layer easily slide along the side between bilayers. [22]

2.2.1 Optical properties

An anisotropic material like the liquid crystal has one or two optic axes depending on the system symmetry. If the light travels into an anisotropic medium, it can be divided into two refracted beams, namely the “double refraction”: an ordinary and an extra-ordinary ray, with polarization parallel and perpendicular to the optical axis of medium, respectively. In uniaxial systems which mean that the media have one optic axis, there are two indices of refraction, n_o and n_e, reflecting the speed of ordinary and extra-ordinary waves respectively. In other words, the two rays propagate with different speeds according to each refractive index. Here the difference n between n_o and n_e ($\Delta n = n_e - n_o$) is defined as birefringence. The origin of birefringence comes from the molecular anisotropy and from the orientational order(S). It has to be considered both what molecular polarizability each molecule has, at microscopic point of view, and what degree of order the molecules possess at macroscopic point of view.

Then, due to Δn of medium, there is a difference of speed between the two rays, and an optical path difference, $\Delta\Lambda = d\,\Delta n$, with d the physical distance travelled by light. Consequently, there is also a phase shift, $\Delta\phi = (2\pi/\lambda)\Delta\Lambda$. This behavior is like in a wave plate, an optical element that changes the state of polarization of light. Therefore in LC samples bright and colorful optical texture can be observed even between crossed polarizers. The color is determined by t the wavelength dependence of the described phenomenon, resulting, for example, in the

disappearing, between crossed polarizers, when a wavelength is coincident with the difference in optical path within the sample. The dependence is shown in a Michael-levy chart where we can deduce sample parameters, birefringence or thickness, from the color and one of the parameters,

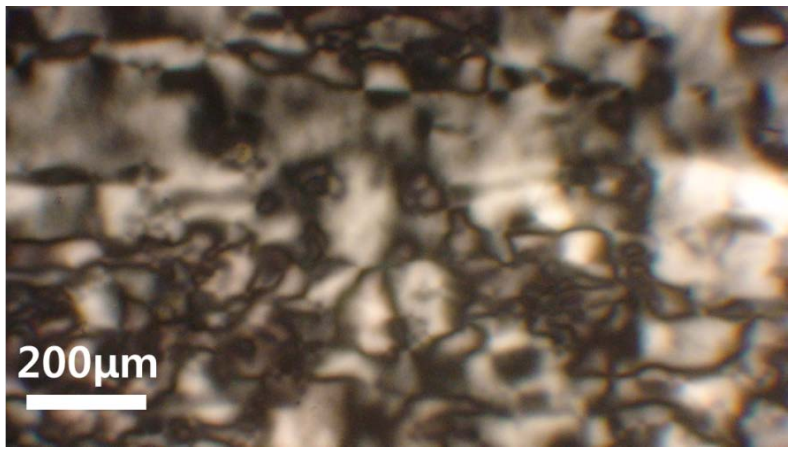

Figure 1 The birefringence image of lyotropic liquid crystal prepared by SDS and 12TAB (ratio=2.5:1) under the polarized optical microscope**.**

As examining the optical texture between crossed polarizers, black regions are often shown as well. One reason is because the refractive index is a function of the direction of propagation of the light with respect to the optic axis. If the light travels along the optical axis as in the homeotropic mode (alignment perpendicular to substrates), the double refraction disappears since n_e tend to n_o, having thus the same value. Or when the direction of light polarization is parallel or perpendicular to the optical axis, completely back parts are also observed because there is only one ray travelling through the medium. For example, the birefringence image of lyotropic liquid crystal is shown in Figure1 as prepared by SDS and 12TAB (ratio=2.5:1) and observed under the polarized optical microscope (POM). POM is normal optical microscopy with crossed polarizers at before and after incident light from lamp passes through the sample. It is useful to optically analyze anisotropic sample at microscopic scale.

Chapter3 Dispersion of carbon nanotubes with the sub-Krafft method

3.1 Sub-Krafft temperature method

The Krafft temperature is defined as the minimum temperature at which surfactant forms micelles. Below Krafft temperature, the excess of surfactant after dispersing CNTs is minimized as crystallized on the bottom (Figure 2B). It have proven to be advantageous for CNT suspensions because it avoids deterioration of properties of CNT and the formation of micelles by which CNT re-aggregates due to depletion attraction.

In a previous work, we used CTAB (cetyltrimethylammonium bromide) as surfactant for the dispersion process, that has a Krafft temperature = 25℃. The process was then uncomfortably performed below room temperature. Here new sub-Krafft procedure is presented using OTAB (octadecyltrimethylammonium bromide) surfactant, belonging to the same family of CTAB, but having a higher Kraft temperature, 38℃, thus allowing convenient process at room temperature. . The molecule structure is shown in Figure2A.

The demonstration of the successful use of OTAB in this study is a demonstration of the generality of the method that can be extended to other types of surfactants needed for dispersing specific nanoparticles. In fact, we can select surfactants with convenient Krafft temperature as occasion demands because Krafft temperature increases with length of hydrophobic chains. If a surfactant with a specific structure is required for a certain process, it is possible to select, within the same family, one with the suitable Krafft temperatures just by choosing homologue with a proper length of chain. Therefore the sub-Krafft method has not limited applicability but the concept can be generalized since other types of surfactants can

be used and also dispersions can be conveniently prepared at room temperature conditions.

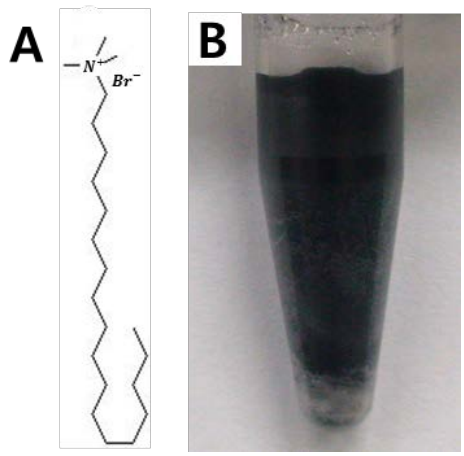

Figure 2 (A) molecule structure of OTAB surfactant and (B) 1mg/ml HiPco SWCNT in OTAB solution prepared by sub-Krafft method. Crystallized OTAB can be recognized at the bottom of the vial**.**

3.2 Method and material

HiPco SWCNTs produced by high-pressure decomposition of carbon monoxide were used. Purified SWCNTs, with an average bundle diameter of ~~0.8-1.2nm and length of ~100-1000nm were purchased from Unidym. The nanotubes contain approximately 5wt% and <15wt% of ash content. Octadecyltrimethylammonium bromide(OTAB) were purchased from Sigma-Aldirch and used as received.

A series of different concentrations of HiPco SWCNT in 1mL OTAB solution (1wt% in DI-W) were prepared: 0.025, 0.5, 0.1, 0.25, 0.5, 0.75, 1.0 mg/ml. The mixture, kept in a water bath for avoiding overheating, was ultra-sonicated by tip sonicator (Hielscher ultrasonics GmbH, UIS250L) using 90 %Amplitude and 0.75 cycle for 30min .To get the sedimentation of excess surfactant, the samples were stored in the incubator at 25℃, temperature that is below the Krafft temperature T_k of

OTAB. As reference, we also prepared samples kept on the hot plate measuring a temperature of 45℃ in the sample. In order to get sedimentation of the excess of surfactant in the below Krafft temperature conditions, typically one week was needed. When white sedimentation is clearly observed like Figure 2B, CNT suspension is carefully took out excluding the crystallized excess of surfactant. Then, the extracted suspensions were centrifuged to remove residual CNT aggregates and large bundles as well as surfactant crystallites (Hanil, Smart R17) at 8000g for 20min at 20°C, for the samples prepared below T_k and at 40°C for the samples above T_k. Same procedures of extraction are carried out at above T_k.

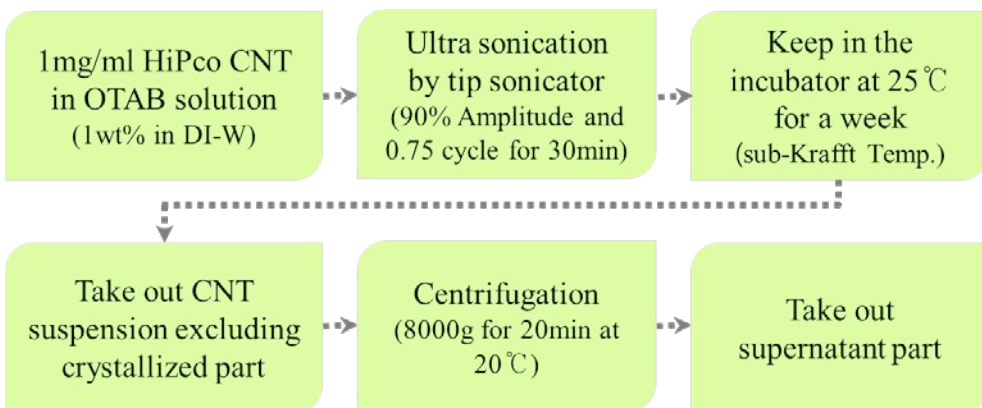

Scheme 1 The scheme of procedure in sub-Krafft method.

The suspensions were analyzed by optical spectroscopy (PerkinElmer, Lambda 35) and by Atomic Force Microscopy (AFM) (VEECO, Dimension® Edge™) in tapping mode.

To deposit individual nanotubes for AFM measurement, we adopted the “bubble method”[23] which is interesting for nanoparticles and tubes due to low cost, simplicity and easiness, independence on type of substrates, ambient condition in comparison with other deposition method. It can be acceptable to deposit mass amount of tubes. We well dispersed CNTs, to deposit not overlapped tubes. CNT surrounded by OTAB molecules between water layers of bubble. The thickness of

bubble layer can be controlled by waiting time since the film thickness decreases with time and consequently the loaded CNT amount contained in the central film area. Controlling the film thickness is thus possible to control the amount of deposited CNTs.

As first, necessary step in the method, surfactant solution should be added to produce a bubble. However, this step is not needed in our case since our dispersed CNT suspension already contains surfactant, OTAB used to prevent CNTs from re-aggregating. We barely managed to make the bubble since minimum amount of surfactant for dispersing CNTs exists in the sample below T_k as compared to the one above T_k which has enough amount of surfactant.

We used 0.1mg/ml CNT suspension in OTAB that was dropped on a substrate forming a bubble. After waiting 1 minute the substrate (1cm X 1cm silicon wafer with silicon oxide) just put to the bubble. Individual CNTs laid on the substrate in extremely thin layer. Sample is placed on the hot plate for a minute to make CNTs strongly adsorbed on the substrate. The substrates were rinsed several times by ethanol and DI-W.

3.2.1 Optical spectroscopy for carbon nanotubes

The electron of molecule absorbs the energy from incident light ranging from ultraviolet to visible and then is excited by the light. Therefore peaks in optical spectra correspond to optical transitions in density of electronic states. In addition, the concentration of solution can be calculated as absorbance value is proportional to the concentration by getting the extinction coefficient from Lambert-Beer law ($A=\varepsilon cl$).

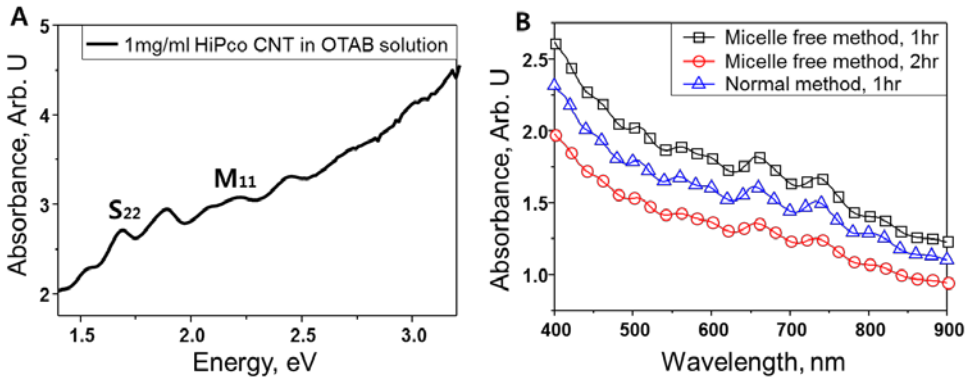

Figure 3 (A) The distinct peaks corresponding to the energy for electronic transition in optical spectra of CNT. (B) Optical spectra of CNT dispersed as various conditions.

The optical spectra of dispersed CNTs are shown in Figure3. CNT spectrum the peaks indicates electronic transitions from valence band to conduction band. For example, in Figure3A, electronic transition from v1 to c1 in density of states of metallic tube is M_{11} where needed energy is approximately equal to 2~2.5eV. The dispersion quality of CNT, furthermore, can be figured out by the more distinct peaks since electronic transition turns up when they are individually detached. The higher absorbance also gives the information for good quality of dispersed tubes because aggregation of CNT goes down to the bottom. In Figure3B the difference of absorbance value among 3 spectra is used criteria for determining quality of CNT dispersion.

3.3 Results and discussion

3.3.1Optical spectroscopy investigations

CNTs concentration can be calculated by their absorbance of the optical spectra. In general, high concentration of CNTs can absorb much larger amount of light, thus

absorbance shows high values. Although samples have nominally the same amount of CNTs, well dispersed suspensions can absorb more light and show higher absorbance values. because CNT bundles, not dispersed during ultra-sonication, go down to the bottom of sample vessel and small aggregates floating in the suspension have nanotubes that can be shielded by the outer ones, resulting in both cases in a reduction in the absorption effect. In other words, well dispersed CNTs are floating without any bundle or aggregation when they are treated with good quality dispersion methods. On the other hand, most of CNTs sink to the bottom and become sedimentation when their dispersion quality is low.

For comparison between above and below T_k methods, we measured the absorbance of CNT suspensions in OTAB solutions at the initial concentrations, when the samples were prepared, ranging from 0.025 to 1.0mg/ml. Before and after centrifugation, the absorbance graphs are shown in Figure 4A, 4B respectively. In both cases the absorbance value becomes higher as the initial concentration of CNTs is increased. Compared with above T_k method (empty symbols with line), the below T_k method (full symbols with line) has higher absorbance in most of the samples.

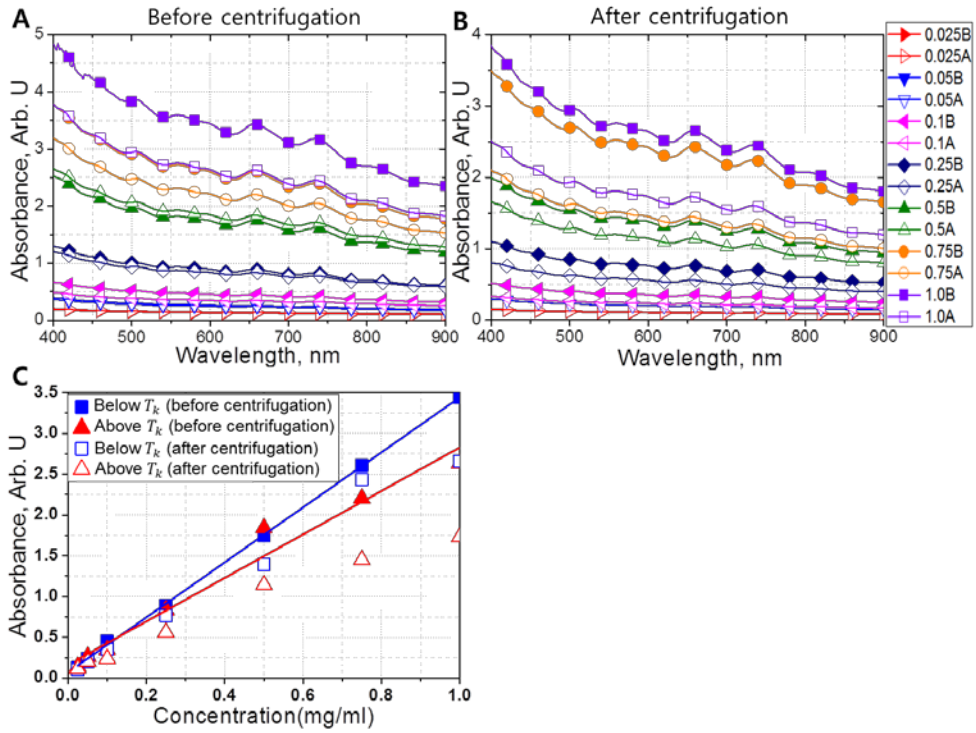

Figure 4 Optical spectra of series of dispersed CNT suspension ranging from 0.025 to 1.0mg/ml comparing above T_k (empty symbols with line) with below T_k method (full symbols with line) (A) before centrifugation, (B) after centrifugation. (C) The absorbance values at 656 nm are reported with respect to the initial concentration of CNTs before and after centrifugation. Symbols are the experimental points and line indicates the linear fit. Squares and triangles indicates the result for below T_k and above T_k respectively.

Theoretically concentration is linearly proportional to the absorbance of optical spectrum according to the Lambert-Beer law:

$$A=\varepsilon c\ell$$

A absorbance, ε extinction coefficient, c concentration, ℓ thickness of solution cell, corresponding to the optical physical path.

The experimental values are reported in Figure 4A, B for the absorbance at 656nm indicating distinct peak of CNT. The results slightly deviates from the linear fitted graphs due to experimental error when plotted as assumption with liner function. In Figure 4C, the error can be confirmed as compared symbols (real results value) and fitted graph lines where extinction coefficients are evaluated as 2.7 and 3.4 at above and below T_k method respectively. This confirms the more effective dispersion with the method at below T_k showing higher extinction coefficient because better dispersion with more individually dispersed CNTs. Indeed in above T_k sample, re-aggregation by depletion attraction reduce absorbance signal since several CNTs are hidden within bundle. In addition, the absorbance of above T_k sample becomes much lower than that of below one after centrifugation, because the large aggregations settle to the bottom, then which is removed by centrifugation.

3.3.2 AFM analysis

We measured deposited CNTs by Atomic Force Microscopy (AFM) to investigate the dispersion quality of CNTs at nanoscale. In comparison with below T_k conditions, a lot of remained surfactant is observed in the above $T_k$sample as expected. A trail of surfactant is clearly shown in the AFM images (compare Figure 5a with 5d). In addition, many tubes formed CNT bundles probably because micelles made by the excess of surfactants induce aggregation via depletion attraction. Figure 5b and 5e are enlarged images from 5a and 5d, which helps the observation of individually dispersed tubes. In the topography images, the height of tubes prepared in above T_k conditions are measured as 2 - 4nm, see Figure 5c, while those from below T_k are typically 1-1.5nm as visible in Figure 5f. The latter values correspond with the written specification of HiPco CNTs. It is obviously shown that the dispersion quality is better with the below T_k method

than with the above one, considering the height of tubes from AFM analysis, indicating lower aggregation into CNT bundles and/ or lower amount of remaining surfactant.

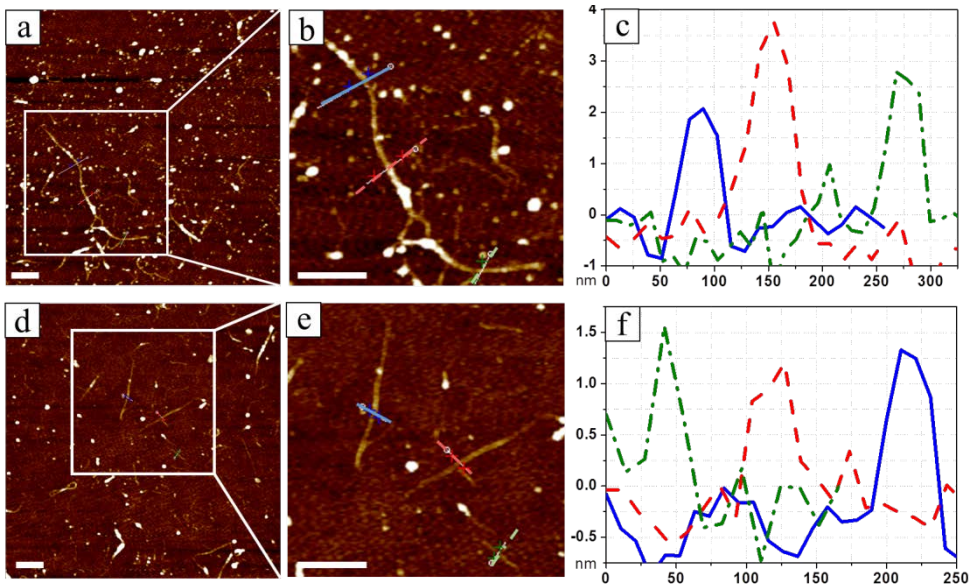

Figure 5 The topography and phase images by AFM for comparing nanotubes deposited from suspensions above T_k(a, b, c) and below T_k(d, e, f) methods. (a), (d) are large area of topography images relatively for checking overall behavior. (b), (e) are topographic zoomed-in from (a), (d) for details. Profile of selected features from (b) and (e) are reported in (c), (f), respectively indicating bundles or tube height. The different style lines correspond to the parts analyzed in the topographic images with the same style line of segments. All scale bars indicate 500nm.

Chapter4 Lyotropic LCs at low surfactant concentration

4.1 Formation of the Lyotropic LC host

As mentioned earlier, amphiphilic compounds can form liquid crystal phases above certain concentration. LC phase can be formed depending on the way a mesogen that is the organizational unit for forming LC, is packed. In general Lyotropic Liquid Crystals (LLC) are formed up at fairly high concentration of building blocks, exhibiting thus viscosity. However, high concentration of surfactant can be a problem in case of LLCs used in some applications such as templates for nanoparticles since remaining surfactant can deteriorate device performance. In this work we aim at forming an LC phase at very low concentration of surfactant. In order to realize this unusual system we look for combinations that can produce extremely anisotropic micelles that easily self-organize. Producing LC phase at as low concentration of surfactant as possible. At this end, we introduce 2 different types of surfactants which possess anionic and cationic headgroups, respectively. The key idea of our designed model is to use electrostatic attraction forces between the positively and negatively charged headgroups of surfactants. [15]

Variation of surface charge is one of the crucial factors to induce transition of micellar shape in LLC system. In case of LLC formed by one type of single chain ionic surfactant at low concentration they tend to form spherical micelles due to repulsion forces between same charges and high surface charge. For the micellar structure to become elongated from spherical to cylindrical shape, an increase in the total concentration of surfactant is required. As the total concentration increases spherical micelles get closer to each other and more packed, then they start to merge together and be elongated for reducing the surface area. This situation is preferred as thermodynamic equilibrium state at the interface water and micelles.

In case of LLC formed by two types of surfactant, on the other hand, when

opposite charged surfactants are mixed, repulsion forces and surface tension are reduced due to charge neutralization. It is more of creating attraction force and decreasing the tendency of curvature formation than changing the surface charge. These make surfactant molecules strung out to form extremely long micelles and better packed, which promote the alignment of micelles along director **n** with long-range order and higher order parameter at even small concentrations as compared with general method of LLC formed by one type of surfactant. Finally this approach enables the formation of liquid crystal phases keeping the surfactant concentration as low as possible.

4.2 Method and materials

The sodium dodecyl sulfate (SDS) and dodecyltrimethylammonium bromide (12TAB) were purchased from Sigma-Aldirch and used as received.

In order to make the lyotropic LC phases powder of SDS and 12TAB are dissolved in water and mixed on the roller mixer at room temperature for 1day, until an homogeneous state was attained. Concentration of whole surfactants leading to the formation of the lyotropic LC phase is only 8wt%. Different molar ratios between SDS and 12TAB were tested evaluating the formation of a lyotropic LC phase. More precisely we have realized the following ratios: 2.3:1, 2.5:1, 2.55:1, 2.6:1, 2.7:1. Those were analyzed by polarized optical microscopy (Nikon, LV-UEPI) with temperature controller (INSTEC, TS62, STC200).

4.3 Results and discussion

We choose SDS and 12TAB, having molecular structures shown in Figure 6, as cationic and anionic surfactants,[24] respectively for self-assembly organization. Due to the same length of hydrocarbon chains they substantially well match with each other. Hydrophobic tails of SDS and 12TAB are at the micelle center while

their head groups with polarity are set toward water. In this system the mesogenic unit is a worm-like long micelle self-assembled by SDS and 12TAB at the molar ratio of 2.5 to 1 at a total surfactant concentration of 1wt%, as result of the combination of oppositely charged surfactants, as reported in the TEM image by Renoncourt. [25]

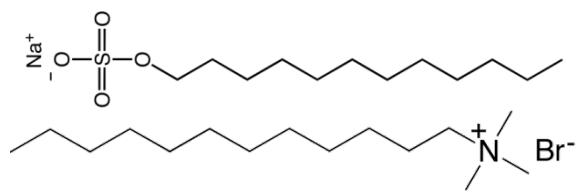

Figure 6 Molecular structures of SDS and 12TAB which have the same length of carbon chain and cationic and anionic headgroup respectively.

We succeed to show the LC phase at a total surfactant concentration of 8 wt% thanks to the ionic combination of molecular charges. This value is very low comparing to conventional lyotropic LC systems that form organized phases usually above 20wt%.

Unlike thermotropic LC, The size and dimension of micelle constituting lyotropic LC changes depending on the phases, which is related to the concentration and temperature and so on. The molar ratio between SDS and 12TAB is important for the formation of lyotropic LC phase due to surface charge changing the micellar size and shape. We have tuned the ratio between SDS and 12TAB to find the ideal value for the formation of the LC phase keeping the overall concentration of surfactant minimized. The ratios that we have considered are: 2.3:1, 2.5:1, 2.7:1. In this way we found that a nematic LC phase was formed for a ratio of SDS to 12TAB equal to 2.5 to 1 as visible between crossed polarizers, whereas for the higher or lower amount of SDS than 2.5:1 an LC phase appears only after shearing, as shown in Figure 7.

Figure 7 Lyotropic LCs, between macroscopic crossed polarizers, formed by different ratios of SDS and 12TAB. (A) 2.3 to 1, (B) 2.5 to 1, (C) 2.7 to 1. The overall concentration, for all samples, is equal to 8wt% in DI-W. (B) The sample strongly shows LC phase but the samples (A) and (C) have only shear induced LC phase.

All three types, prepared with different ratios, were filled into capillaries applying some kinds of shearing force by a syringe pump. Using polarized optical microscopy, the 2.5:1 sample still exhibits striking birefringence confirming LC properties. Instead, the sample formed with the ratio 2.3:1 does not show any bright texture as visible in Figure8, thus not exhibiting any birefringence. Finally, the 2.7:1 sample shows optical property of LC phase as result of the flow-induced alignment obtained by injecting it into the capillary. Even though the 2.3:1 samples got shearing force from capillary injection, that was not enough to align the micelles, unlike for the 2.7:1 samples. These results mean that small ratio differences can strongly influence the formation of the ordered phase, whether spontaneously appearing or under shearing.

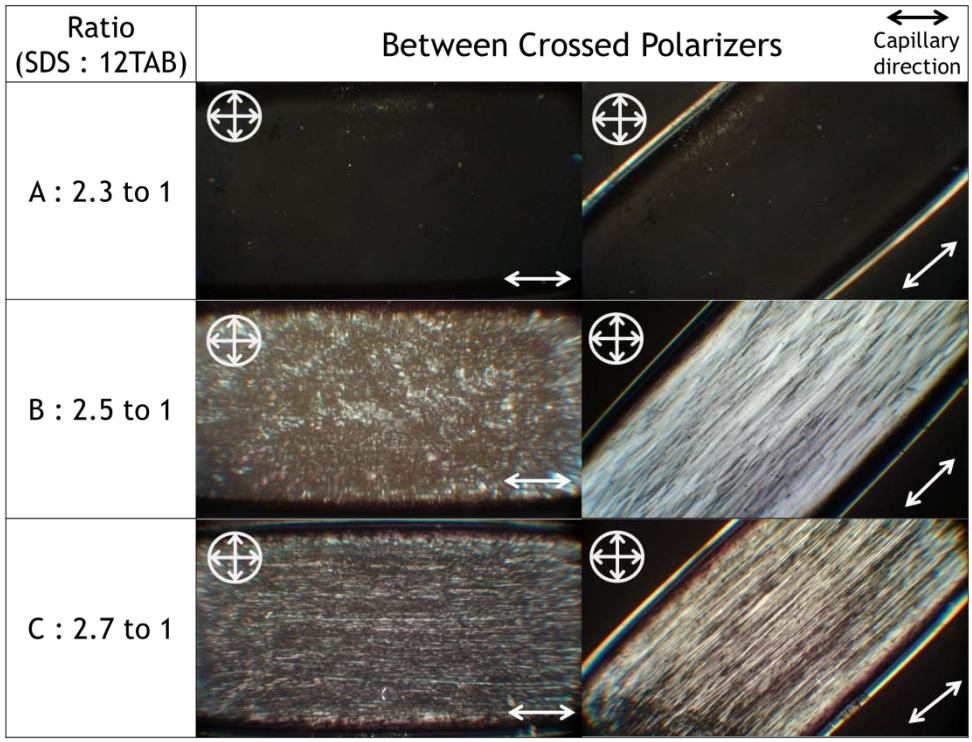

Figure 8 The optical images between crossed polarizers of lyotropic LCs filled into capillaries (0.1mm x 2mm). The mixtures were prepared with different ratios of SDS and 12TAB ; (A) 2.3 to 1, (B) 2.5 to 1, (C) 2.7 to 1

Temperature affects the phase transition although in the general definition of lyotropic LC this is mainly connected to the concentration. It is because the solubility of the solute changes depending on the temperature of solvent. Although in normal lytropic LC the influence of temperature is marginal and in general ignored, interestingly, our LLC system has a significant response to temperature even for few degrees of difference.

First, we briefly checked phase transition temperature between macroscopic crossed polarizers for intuitive observation after heating vials up on hot plate. Figure9 clearly shows how the phase is changed as consequence of the temperature change. We can macroscopically observe the change of the LC phase in particular in samples (2) and (3) while sample (1) doesn’t show any birefringence all range of

temperature. In case of sample (2) striking LC phase was presented for a broad range of temperature near room temperature (RT) and then observed absent at 42.2℃. In Sample (3) LC phase appeared below RT while at RT the LC phase is only shear-induced. This phenomenon indicates that the effect of temperature is quite considerable in our system even they are lyotropic LCs.

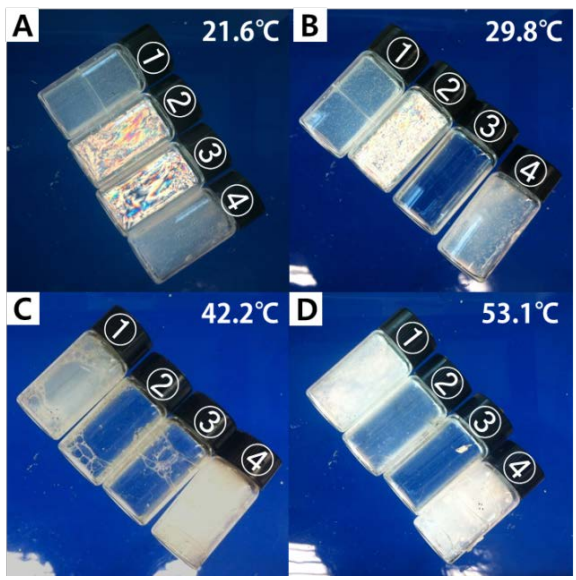

Figure 9 The change of LC phase as temperature increases from 21.6℃ to 42.2℃, observed between crossed polarizers. The ratio between SDS and 12TAB of samples are equal to (1) 2.3: 1, (2)/(4) 2.5 : 1, (3) 2.7 : 1. In case of (4), OTAB solution, which is same solution used in CNT dispersion, is added to the sample with 2.5 ratio.

Then, those samples were filled into capillaries for measurement specifically devoted to the study of phase transition behavior by polarized optical microscopy in combination with a temperature controlled stage. As observed 3 samples, birefringence textures of them have different trend near the phase transition temperature. Figure 10 shows the phase behavior of all samples near range of phase transition for each sample. In case of 2.3 :1 and 2.5 : 1 samples, some parts

disappeared nematic phase or made droplets as shown in Fiugre11A and B as temperature increased until reached around phase transition temperature. On the other hands, the texture continuously disappeared at same procedure. In the framework of a collaboration with the University of Kyoto in Japan we are using Dynamic Light Scattering (DLS) for investigating the type of phase transition occurring. The average size of micelles was roughly calculated from relaxation time caught by DLS measurements. During phase transition the size of micelles was constant in case of 2.3:1 and 2.5:1 samples while the size was elongated in 2.7 samples. This result can suggest that the driving force in the transition from isotropic to nematic region is the alignment of micellar director in 2.3:1 and 2.5:1 samples and elongated micelle in 2.7:1 samples. The scheme of this phenomenon is shown in Figure10D

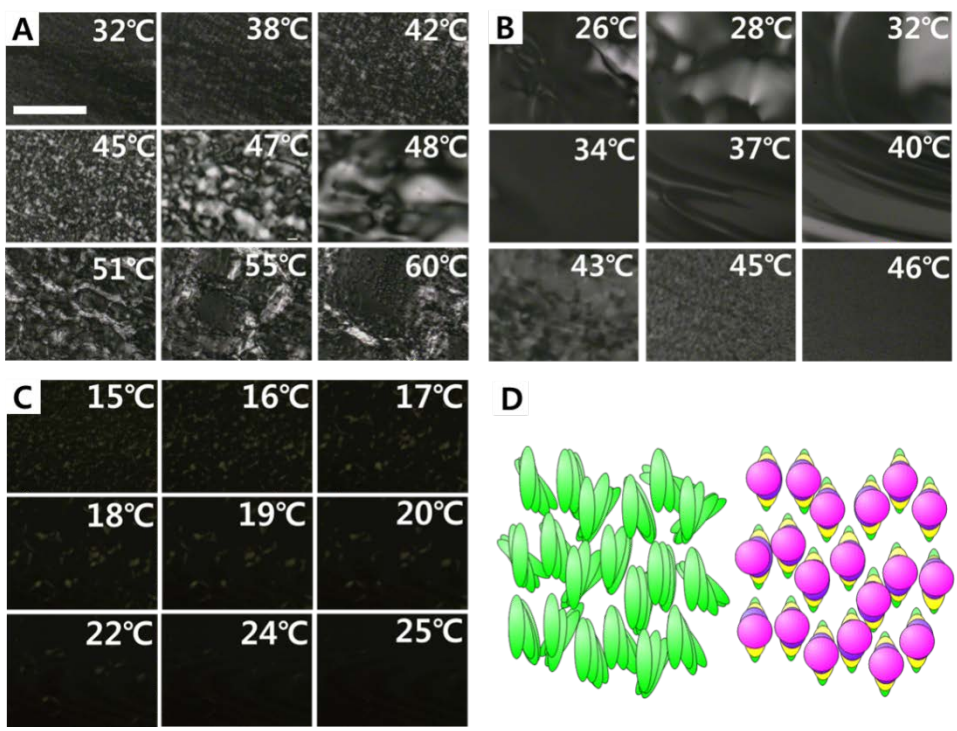

Figure 10 Polarized optical microscope images of LLC samples with ratios (A) 2.3 to 1, (B) 2.5 to 1, (C) 2.7 to 1, filled into capillaries for measurements of phase

transition behavior. (D) The scheme of micelle shape change as effect of temperature change around the phase transition temperature. The scale bar indicates 500μm.

Chapter5 LC-CNT composite

5.1 Aligned CNTs by lyotropic liquid crystal host

We have already discussed the importance of aligning CNTs as part of our motivation. In order to achieve maximum performance of CNTs profiting by their superb properties, alignment should be ultimately realized into a specific direction and be controlled since, in anisotropic materials, the characteristics between longitudinal and transverse directions are completely different.

LCs have attracted attention as attractive host materials due to their unique advantages such as anisotropic configuration and fluidity, straightforward organization due to the self- assembly. Transferring their orientational order to guest particles produces alignment even at nanoscale. In particular, lyotropic liquid crystals (LLC) are ideal for obtaining higher load of CNTs than thermotropics and still obtaining unidirectional alignment. In addition, one of the key advantages is that, since host material should be ultimately eliminated for device to be used commercially. lyotropic LC can be more easily removed[13, 14] after finishing its role compared with thermotropic LC. Here, our key idea is to use a LLC formed by very low amount of surfactant as aligning host for forming an ordering template but minimizing the surfactant content. In this way CNTs can benefit from the templating action of LLC while preserving as much as possible their pristine properties due to the very low amount of the host.

5.2 Method and materials

1mg HIPCO SWCNTs in 1wt% OTAB was made by Krafft temperature(25℃) method as described in Chapter 3. In order to make the lyotropic LC phases powder of SDS and 12TAB was prepared aiming at a total concentration equal to 8wt%. SDS and 12TAB were mixed testing 3 different molar ratios; 2.3:1, 2.5:1,

2.7:1 of SDS:12TAB, the same as in Chapter 4.

Powders of SDS and 12TAB were mixed with CNT suspensions prepared with the sub-Krafft method. The amount of the CNT suspension was half of the one of water used for the preparation of the LC phase solution formed by SDS and 12TAB. First, powder of 12TAB was added into the dispersed CNT suspension and the mixture was kept on the stirrer with magnetic bar for 20min. s 12TAB molecules are easily dissolved since their molecular structure is similar to that of OTAB, used for dispersing CNTs. SDS solution is added to this mixture, combining with the dissolved 12TAB molecules not only forming the LC host but also allowing CNTs to be incorporated in the LC host. It is important, after dissolving SDS in water and 12TAB in the CNT suspension, respectively, to mix them thoroughly in order to well disperse CNTs in the host and facilitate their alignment along the LC director. Afterwards the sample was ultra-sonicated at the same conditions as previously discussed for a better incorporation and homogenization. The final suspension was filled into flat capillaries with cross sections equal to 0.1 x 1mm or 2mm and produced the filament for alignment of CNTs as pulled by shearing force. This fiber was freeze-dried for 1 day after treated by liquid nitrogen. Those were analyzed by polarized optical microscopy (Nikon, LV-UEPI) and polarized Raman spectroscopy (Dongwoo optron, Raman set-up) with Argon ion and He-Ne lasers.

5.2.1Polarized Raman Spectroscopy

Raman spectroscopy analyzes properties of samples using inelastic scattering phenomena. There are three types of scattering phenomena depending on the energy difference between incident and scattered photon. When the energy of the photon is the same after the interaction with the sample, this is an elastic scattering known as Rayleigh. When the molecule emits lower or higher energy, those are inelastic scattering processes, called Stokes and anti-Stokes, respectively. The signal in Raman spectroscopy is acquired from Stokes and anti-Stokes scattering.

A laser beam is scattered after interacting with the material. The energy of the scattered radiation is changed as consequence of the light-matter interaction. In case of Stokes scattering, the energy absorbed induces electronic transitions to higher excited states that can be also virtual states. From this state electrons reach then a lower energy state, transferring the energy to vibrational or rotational modes, and from this they can relax to the ground state emitting photons at lower energy than the incoming ones In the anti-Stokes scattering the emitted photon energy is higher than the incoming one because the original state of the electrons is not the ground state. In general numerous electrons exist in the ground state, more than in higher excited states. Therefore the signal from Stokes scattering is stronger than the anti-Stokes. The energy difference between detected signal and source is related to characteristic vibrations of molecule or of solids, appearing as specific peaks in the Raman spectra.

Raman spectroscopy is a very useful technique for carbon materials and for carbon nanotubes in particular due to their specific, thus recognizable, Raman spectrum, and for the resonance phenomenon. In fact, typical laser wavelengths correspond to the energy of electronic transitions in carbon nanotubes, allowing to acquire the Raman spectrum of even one individual CNT, It is useful for estimating if the tubes are metallic or semiconducting, for various analysis such as deformation, chirality, , doping, evaluation of diameters, but also for graphene like for establishing the number of graphene layers, when the number is law.

The main modes for carbon materials are D, G and 2D-bands which are roughly around 1350, 1580, 2700 cm^{-1} respectively. The Radial Breathe Mode (RBM) is typical for carbon nanotubes and the peak position is dependent on the nanotube diameter.. D-band is a dispersive band and often used for assessing the disorder or defects in the graphitic structure by doing the ratio with the G-band. In CNTs the G-band is associated with tangential modes, consisting of two peaks, G+ at 1590

and G-1570, which can be used to distinguish between metallic and semiconducting CNTs. [26]

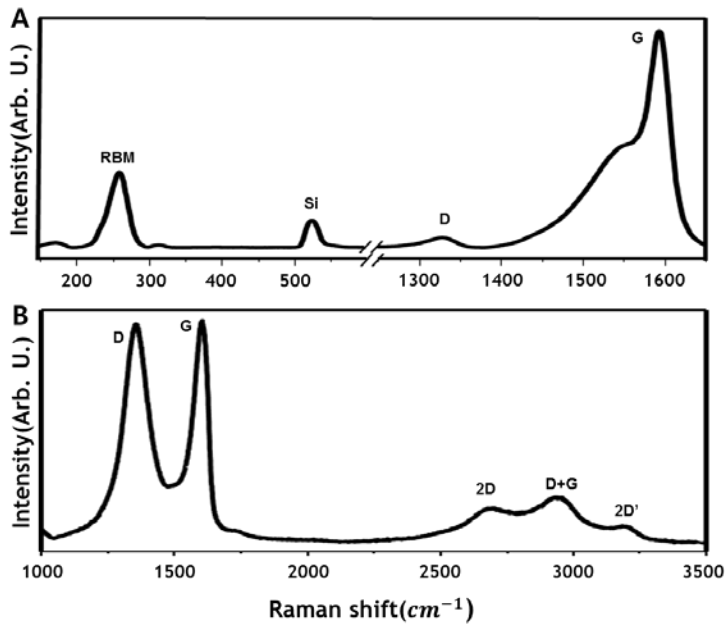

Figure 11 (A) Raman spectra of HiPco SWCNT and (B) graphene oxide with 514.5nm laser wavelength.

We give an example of spectrum of SWCNTs in Figure 11A with peaks like RBMs and the G-band well recognizable, In Figure 11B the spectrum of graphene oxide with the high D and G-band along with the 2D, 2D peaks along with the D+G due to defects induced by oxidation.

We have used a polarized Raman spectroscopy based on a micro-Raman set-up equipped with polarizer set-up for analysis of anisotropic materials.[27] An half-wave plate is used to rotate the input light polarization and another polarizer is placed during the light path after interaction with the sample. An element for depolarizing the light is also inserted to avoid artifacts due to polarization sensitive effects in the final detection stage, The advantage of this set-up is that the polarization direction of incident light can be adjusted just by rotating the wave

plate obtaining rotations from 0º to 90º. For example, when the wave plate is rotated as 45º the direction of polarized light is turned of 90º. It is valuable to measure the effect of the direction of the polarized light at the exactly same spot, impossible with the systems that keep the polarization of light fixed while the sample is rotated. The simple scheme of polarized Raman spectroscopy set-up is shown in Scheme 2.

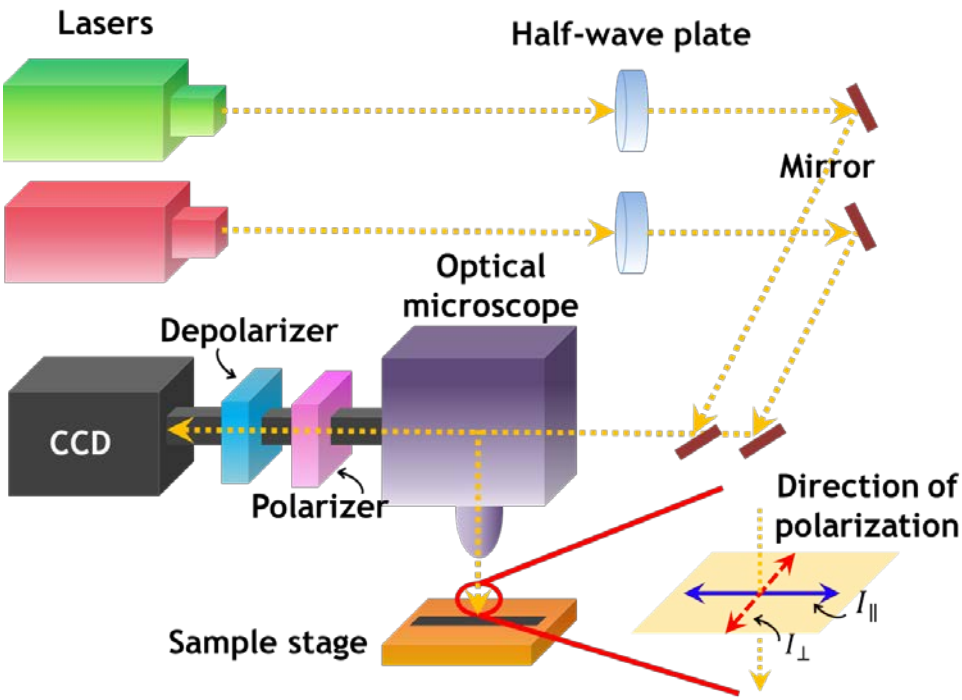

Scheme 2 The scheme of polarized Raman spectroscopy set-up

5.3 Results and discussion

5.3.1Effect on LC phase by CNTs

LC-CNT composite is investigated in capillaries by optical microscopy as shown in Figure 12.

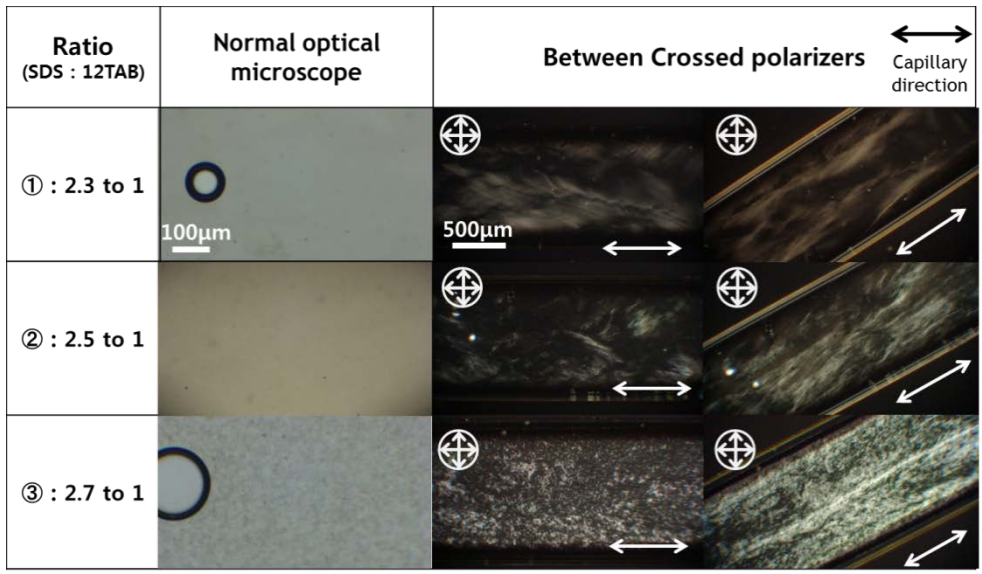

Figure 12 LC-CNT mixtures formed with different ratios of SDS and 12TAB, (1) 2.3 to 1 and (2) 2.5 to 1 and (3) 2.7 to 1. They are filled into flat capillaries imposing shear force.

For our composites CNT aggregation was usually not optically detectable which means that aggregates, if present, are below optical resolution, Thus CNTs, surrounded by OTAB molecule, are kept dispersed and incorporated in the lyotropic LC as shown in normal optical microscope images, left of Figure 12. In case of 2.7:1 sample, however, there are many aggregates of CNTs. The reason can be due to the higher ratio of SDS compared with 2.3:1 and 2.5:1 samples. SDS has negatively charged headgroups and an increased amount can attract more strongly the OTAB molecules surrounding CNTs, which have positively charged headgroups. Then, if OTAB molecules leave the surface of CNTs, those would then tend to reaggregate.

LC host has the tendency to align along capillary direction when it is filled into capillaries and especially when imposing a stronger shear flow. CNTs align along the direction of the LC host, as indicated by the occurrence of birefringence also in

the composite, right images in Figure 12. In fact the overall capillary is brighter when rotated at 45º between crossed polarizers.

CNT affect also the behavior at phase transition, helping to retain the order of LC host above the pristine phase transition temperature, when the lyotropic LC changes from nematic to isotropic phase. We checked the phase transition temperatures before and after adding CNTs into lyotropic LCs. Some lyotropic LC samples show a complete isotropic phase at relatively low temperatures. These samples are the ones with ratios of SDS and 12TAB equal to 2.7: 1, 2.6:1, 2.55: 1.The samples with ratios equal to 2.5:1 and 2.3:1 were excluded because they present nematic-isotropic phase coexistence even at a quite high temperature.

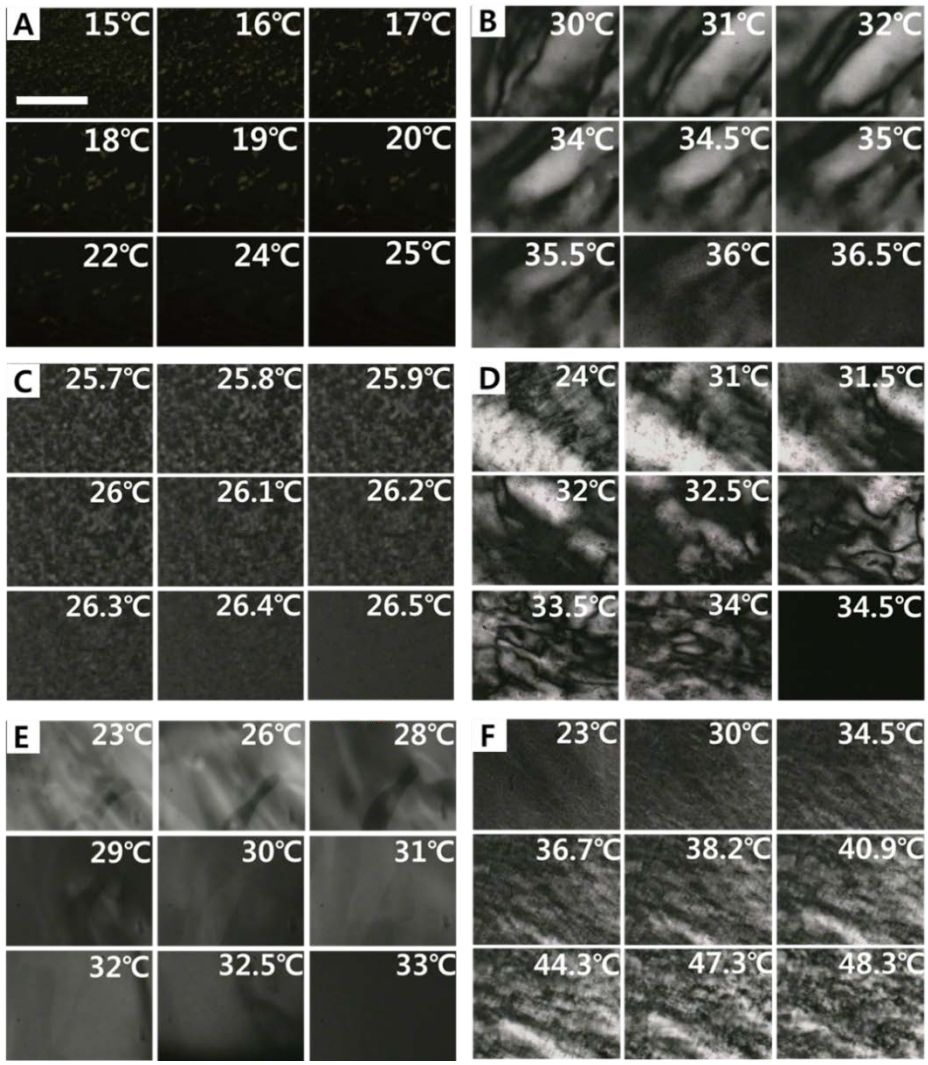

Figure 13 The phase transition temperature between nematic and isotropic phase changed by adding CNTs in samples with ratio 2.7: 1(A, B), 2.6:1(C, D), 2.55:1(E, F). The samples were heated in a hot stage during the optical microscope investigations. The images (A), (C), (E) are of the pure LC phase and (B), (D), (F) for LC samples doped with CNT. The scale bar corresponds to 500μm.

In case of the sample with ratio 2.7:1, it exhibits completely isotropic phase at 25℃ upon temperature increase, as shown in Figure13A. After adding the CNTs,

however, the transition temperature between nematic and isotropic moved to 36.5℃ as shown in Figure13B. Likewise, in Figure13 2.6:1(C, D) also display the same tendency to rise the phase transition temperature by approximately 10℃. Furthermore, 2.55:1(E, F) sample maintains LC phase within controlled temperature range. The increase of phase transition temperature can be related to an increase of order in the LC host, which is compatible with the observations reported earlier regarding the spontaneous appearance of LC phases in doped samples while the pristine showed only shear-induced LC phase. The changes of phase transition temperature for each sample before and after adding CNTs are rearranged in Table 1.

Table 1 The changes of phase transition temperature for each sample before and after adding CNTs

Ratio(SDS:12TAB)	2.7:1	2.6:1	2.55:1
Pure LC state	25℃	26.5℃	34.5℃
LC doped CNTs	36.5℃	33℃	Above 48.3℃

5.3.2 Effect of OTAB on the composites with time

We have monitored the behavior of the LC-CNT composite in time for evaluating its stability t. A day after filling the capillary with the samples, we re-watched same capillary which is used at image of section 5.1.2.

In Figure 14A, B there are whitish spots visible both without and between crossed polarizers, indicating that these areas are birefringent. The rest appears still uniform indicating a still good dispersion of CNTs since CNT aggregation is still not

detected. However, it is an indication that LC-CNT composite is phase separating or it is somehow changing. However, despite some bright spots are clearly visible, suggesting the presence of a LC phase without CNTs, a complete phase separation was not observed and large portions appear still with uniform distribution of dispersed CNTs and still birefringent. Therefore the possible separation process seems to be quite slow or limited in the capillary.

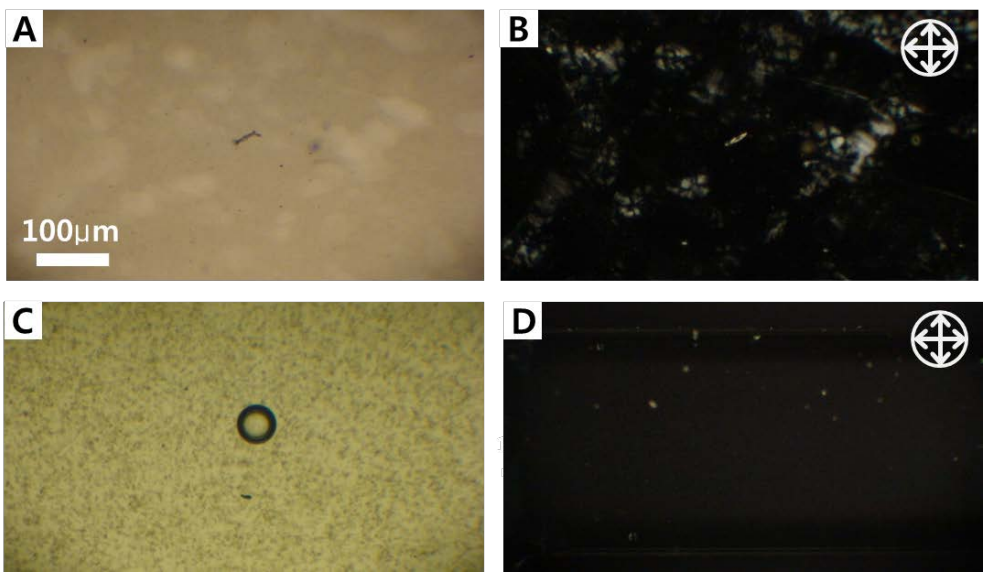

Figure 14 Optical microscope image of (A)same capillary with 2.5 : 1 sample, as in sample 1 of Figure 12 one day after filling, (B) under the polarized optical microscope and (C) 2.5 : 1 sample filled into the capillary a day after the preparation of the LC-CNT mixture,(D) under the polarized optical microscope.

Another experiment was done preparing the sample, letting it stand for one day and then filling a capillary. We observed many aggregate of CNT and no birefringence as shown in Figure14A, B. As time goes on, this tendency becomes worse. Our explanation is that CNTs are deprived of OTAB surfactant that can be attracted by the negative charged SDS. Then, without surfactant, CNTs aggregate OTAB molecules that leave CNTs are mixed with LC host and they can interfere with the

LC formation for, at certain surfactant ratios for the LC. In sample 4 of Figure 9, we verify that OTAB can suppress LC phase since there is no noticeable birefringence between crossed polarizers when 1wt% OTAB solution, instead of just water, is added in lyotropic LC made by ratio of SDS and 12TTAB equal to 2.5:1.

Our observations corroborate the peculiar nature of our system and the importance of proper balance of the components to find the suitable ratio for preserving the phase as well the good dispersion of CNTs in time.

5.3.3 Characterization by Polarizer Raman spectroscopy

The addition of CNTs in the LLC has also an effect on other properties of the host like the viscosity. It becomes also easy the creation of filaments from lyotropic LC-CNT composites, being formed by just dipping and pulling out a sharp object such as a needle, as shown in Figure15A. When the filament is pulled out, micelles constituting LC phase assemble themselves along the filament direction by pulling force. At the same time CNTs incorporated into LC phase spontaneously follow the direction of LC assembly meaning that CNT rods align in between micelles forming the LC phase, thus along the fiber axis.

This is a valuable property of this composite for realizing CNT alignment due to the self-assembly of LC and useful having an easy control of the deposition as fibers can be simply produced.

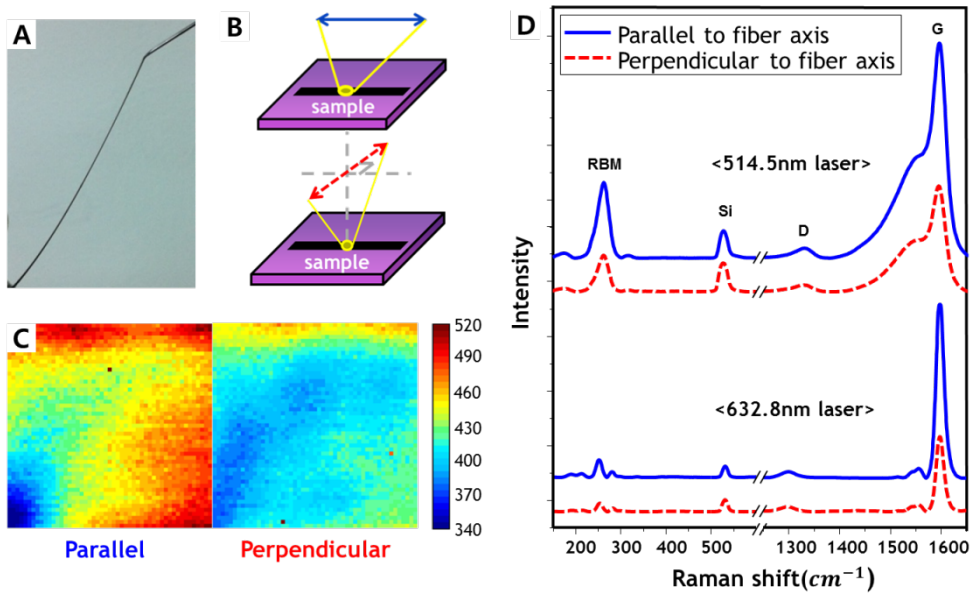

Figure 15 (A) Easily produced filament from LC-CNT composite for aligning CNTs along the fiber direction. (B) Scheme of the directions of fibers and polarization of incident laser. The upper one (solid line) is the polarization direction of incident laser parallel to the fiber axis and the bottom one (dotted line) is perpendicular. (C) Raman mapping images of G-band using the two perpendicular directions of light polarization. The size of the scanned area is 50μm X 50μm for checking the presence of macroscopically ordered domains. (D) Raman spectra of aligned CNTs measured with two perpendicular directions of light polarization. Two type of lasers were used, 514.5nm and 632.8nm laser wavelengths.

The CNT alignment can be recognized with anisotropic measurements, like with polarized Raman spectroscopy. The polarizability of CNTs is much higher along the tube axis than perpendicular to it, which is reflected in the difference in the intensity of the Raman modes when light with polarization parallel and perpendicular to the tube axis, is used. Therefore we checked the alignment of CNTs deposited on substrates by the process of pulling the fiber. We used two polarization, parallel and perpendicular to the fiber axis, as shown in the simple

scheme of Figure 15B. The upper one represents the polarization direction of the incident laser parallel to the fiber axis while the bottom one is perpendicular to it.

Then we measured the Raman spectrum for the two input polarizations, collecting the scattered signal with the same polarization as the incident light. Because the nematic phase is not perfectly ordered even if has orientational order with the preferential direction denoted by the director **n,** the intensity of the peaks for light polarization perpendicular to the axis cannot totally vanish. The clear difference in the intensity of the Raman peaks measured for the two polarizations, however, still unambiguously discriminate the occurrence of an average aligning direction, with the peak intensity $I_{\parallel}$ much higher than $I_{\perp}$, for RBMs and G-band, as shown in Figure15D. To be more quantitative we calculate the order parameter S,[11] which gives the degree of order of the phase and becomes 1 for crystals and 0 for isotropic liquids. Introducing the Raman dichroic ratio D,

$$D = \frac{I_{\parallel}}{I_{\perp}}$$

The nematic order parameter S becomes:

$$S = \frac{D-1}{D+2}$$

For our system the evaluated value of S is between 0.25 and 0.3, depending on the choice of the peak. This result denoted that CNTs in this system were indeed aligned with an order parameter S～0.25-0.3- Although the value is not very high it still indicates the presence of a nematic phase. Possible reasons of the reduced measure value of S can be associated to the lyotropic system that might need higher shearing forces for better alignment or it can be a consequence of the drying process used after the deposition of the fibers to remove the water. Even if we used freezer dryer for removing the water, the pretreatment with nitrogen could have

been not fast enough to prevent movements of the tubes as effect of the water removal.

Finally we measured intensity of G-band in a large area by using the mapping function, still for the two perpendicular polarization of light, in Figure 15C in order to prove that the alignment is realized not only at a certain point but also on a large scale. The size of the chosen mapping area is 50μm X 50μm, to observe ordered macroscopic domains. The intensity of the peaks for light with polarization parallel to the fiber axis is in all points higher than the intensity for the perpendicular polarization, demonstrating that the nanotubes are aligned, on the average and in the all area, along the same direction. This is a demonstration of the successful transfer of unidirectional order even in the case of a matrix with very low surfactant content.

Chapter6 Lyotropic LC phase of Graphene oxide

6.1 Synthesis and characteristics of graphene oxide

To produce graphene we have been interested exclusively in the solution-based approach which is based on chemical exfoliation. There are two ways can be used by exfoliation of graphite: 1) the direct exfoliation of graphite via sonication in organic or water/surfactant solutions and 2) the oxidation of graphite followed by the exfoliation of graphene oxide. The first approach presents the advantages to conduct easily to graphene nanoparticles; the evident drawback comes from the harsh sonication condition used to produce the material. Indeed, the graphene flakes obtained via this technique are very small (less than 1 μm in general). The oxidation of graphite leads to graphite oxide which exfoliates spontaneously in large graphene oxide flakes (usually more than 40 μm - several hundreds of μm^2). We chose the second one and followed a procedure derived from the so-called Hummer's method. [28] At the end of the oxidation, the Graphene Oxide (GO) flakes are separated by centrifugation and no sonication step is performed. Graphene oxide suspension obtained by the following method consists of mainly large flakes.

6.2 Method and materials

Natural expandable graphite was purchased from Qingdao xinghe graphite co., Ltd. Hydrogen peroxide solution, sodium nitrate, potassium permanganate, sulfuric acid, tetrahydrate 5,10,15,20-Tetraphenyl-21H, 23H-porphine-p,p′,p″,p‴-tetrasulfonic acid tetrasodium hydrate was purchased from Sigma-Aldirch.

Polarized optical microscopy (Nikon, LV-UEPI), optical spectroscopy (PerkinElmer, Lambda 35), fluorescence spectroscopy (Scinco, FS-2) were used for analysis.

6.2.1 Synthesis of GO

1g of natural expandable graphite powder was added in round-bottom flask. Graphite as fundamental basis determines the properties of the resulting suspension. Expandable graphite is suitable for synthesizing large graphene oxide (GO) flakes because it exfoliates into GO more easily than normal graphite. 1g of $NaNO_3$ (powder) as strong oxidant was added into a flask. 48ml of H_2SO_4 (96%) was slowly added by using a pipette. The preparation should be performed keeping the flask surrounded with ice bath, keeping the temperature at 0℃ in order for reaction to be moderate. The flask was put on the magnetic stirrer with the magnetic bar as speed of 400rpm. 6g of $KMnO_4$ (powder) as strong oxidant was slowly added and stirred for 1hr 30min. Ice bath was also used here to keep the temperature of reaction at around 0℃ because a lot of heat is produced when $KMnO_4$ is introduced in the reaction. The color of the mixture changed from purple to green, due to the formation of Mn_2O_7 which is the oxidant of the graphite.

$$KMnO_4(s) + 3H_2SO_4(l) \rightarrow K^+(aq) + MnO_3^+(aq) + H_3O^+(aq) + 3HSO_4^-(aq)$$

$$MnO_3^+(aq) + MnO_4^-(aq) \rightarrow Mn_2O_7(s)$$ [29]

The reaction was then agitated for 2 hr at 35℃. 40ml of distilled water were very carefully and slowly added during 30min keeping the ice bath because it is dangerous to add water in strong acid. In general, we should add strong acid into the water to prevent from violent reaction. 100ml of distilled water was added into the diluted mixture. Then additional 5ml of H_2O_2 was added to remove unreacted oxidant MnO_2. Many bubble were formed and the color of the mixture became lighter than before because MnO_2 (brown powder) is reduced into Mn^{2+} by H_2O_2.

$$2MnO_2\ (s) + 5H_2O_2\ (l) + 6H^+\ (aq) \rightarrow 2Mn^{2+}(aq) + 3O_2\ (g) + 8H_2O\ (l)$$

At the end of the reaction, the mixture was transferred in tubes for centrifugation. The supernatant part which includes Mn^{2+} and H^+ was removed after centrifugation at 15000rpm for 10min. This procedure is repeated 6 times. In order to check if

Mn^{2+} ions are still present in the mixture, since we know that by adding sodium hydroxide (NaOH), and sodium sulfide (Na_2S), if there is still Mn^{2+}, white or brown salt becomes visible.

$$Mn^{2+}(\text{aq}) + NaOH\ (\text{aq}) \rightarrow Mn(OH)_2\ (\text{white})$$

$$Mn^{2+}(\text{aq}) + Na_2S\ (\text{aq}) \rightarrow MnS\ (\text{brown})$$

After this treatment, the pH of the solution reaches 4~5. At this stage the suspension is clearly visible as divided a gel structure in the upper and precipitate on the bottom. The mixture is then centrifuged at 5000rpm for 10min in order to eliminate the biggest particles of graphite/graphite oxide. The gel is collected and the procedure is repeated again until gel state disappears. The gel is in fact the suspension of individual flakes of graphene oxide in water, probably in a nematic phase. The final GO suspension is shown in Figure 16A

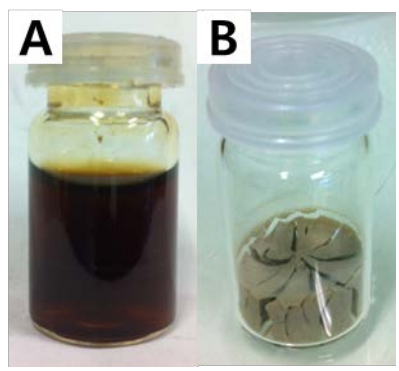

Figure 16 (A) GO suspension (2.5mg/ml) after synthesis and (B) freeze dried sample for the concentration determination.

Lyophilization step by freeze dryer is useful to know the concentration of synthesized GO suspension which is necessary for checking threshold concentration in liquid crystal phase. The water in the suspension is eliminated by sublimation at low pressure, below 0.05mbar, and at a temperature ~ -50°C. The sample was pretreated, putting it into liquid nitrogen in order to be quickly frozen such that water gets into an amorphous state. In fact normal ice, unlike the frozen amorphous state, occupies larger volume than the liquid phase because of its lattice

structure. With the sample pretreatment, we avoid interference of crystallized ice with the order of the GO structure. Sublimation is also useful to avoid capillary bridges arising during water evaporation that can induce aggregation between flakes. Having ice around the sample has also practical consequences since it makes easier to know when the process in the freeze dryer is over, that means when the ice disappears. The sample is nevertheless let overnight in the freeze dryer to eliminate all possible traces of water. The dry sample of GO, shown in Figure 16B, is measured for weight and we could determine that our original gel contains 2.5mg/ml of graphene oxide.

6.2.2 GO/Chromophore mixtures

The sodium salt of the meso-tetrakis[4'-(sulfonatophenyl)]porphyrin was used for negatively charged porphyrin.

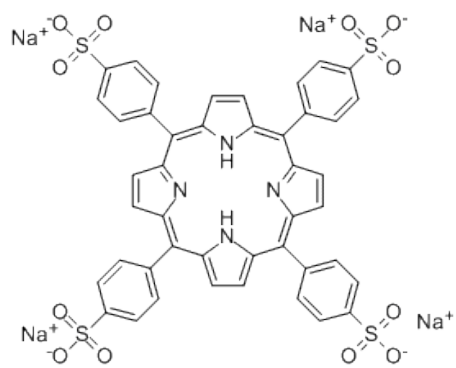

Figure 17 The molecule structure of $SO_3^-Na^+$-porphyrin (5,10,15,20-Tetraphenyl-21H, 23H-porphine-p,p′,p″,p‴-tetrasulfonic acid tetrasodium hydrate) which we used in the Chapter7.

We prepared graphene oxide/porphyrin mixture and a reference sample with just GO-Negatively charged porphyrin ($SO_3^-Na^+$-porphyrin), is prepared with a concentration of 0.0025mg/ml in water. The graphene oxide/$SO_3^-Na^+$-porphyrin mixture is mixed keeping the same overall concentration of the reference sample.

The ratio between GO and $SO_3^-Na^+$-porphyrin in this mixture is equal to 250:1 (0.25mg/ml of GO and 0.001mg/ml of $SO_3^-Na^+$-porphyrin).

6.2.3 Reduction of GO and rGO/Chromophore mixtures

The reference and graphene oxide/$SO_3^-Na^+$-porphyrin mixture samples were freeze-dried and then heated at 150°C under low pressure of CO for 24h. This method of reduction was chosen because it did not require the use of any liquid reducing agent like hydrazine or sodium boron hydride that leave always traces of chemicals after the reduction steps. [30]

The reduced GO (rGO) material was not anymore soluble in water after this treatment since graphene, like carbon nanotubes, is hydrophobic. Therefore a part of rGO/$SO_3^-Na^+$-porphyrin hybrids were dispersed in an organic solvent (*N*-methylpyrrolidone - NMP).

6.3 Results and discussion

6.3.1 Evaluation of the flake area

To measure the size of graphene oxide (GO) flakes that we synthesized, imaging by scanning electron microscopy (SEM) was carried out after deposition of the flakes on silicon substrate. Since the strategy used to deposit GO as uniform monolayer is crucial for a clear observation, the bubble method[23] described in chapter X, based on the deposition of nano-object incorporated in water/surfactant films, is chosen also here This method permits to deposit GO in an unfolded and unwrinkled manners. Several factors for the successful bubble deposition method should be considered such as the time of drainage after making the bubble, initial concentration and amount of suspension to make the bubble and the bubble size.

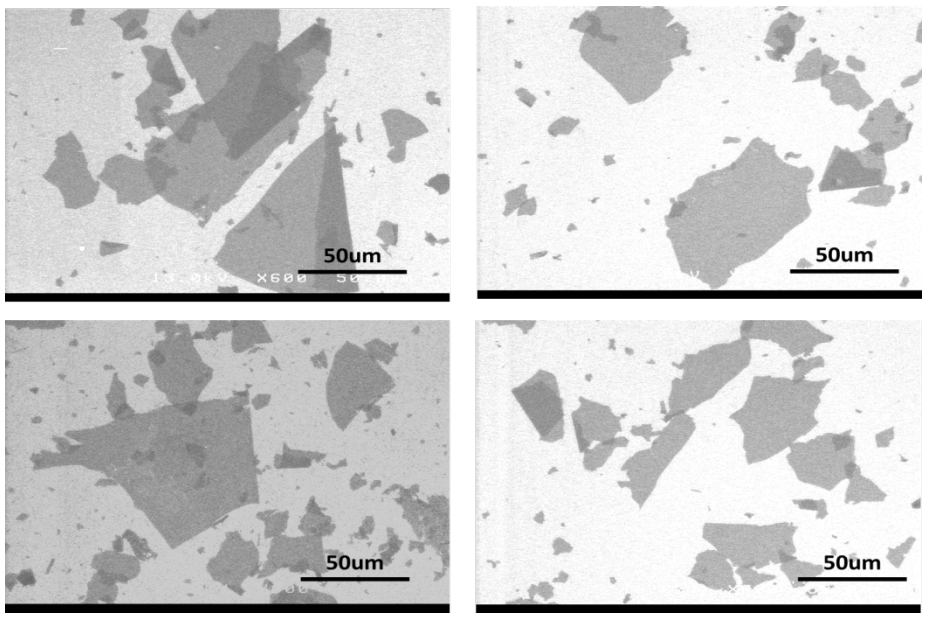

Figure 18 Deposited GO sheets on Si/SiO_2substrate. It is evident that extremely large flakes can be produced with our method.

Figure18 shows GO flakes deposited on Si/SiO_2 surface; the substrate appears in white/grey, the light gray objects are monolayers of GO and the darker area are due to overlapped of folded GO flakes. We can observe that the flakes are fairly large monolayer GO sheets and their diameters reach around 50 m. The image shows also the presence of small flakes with diameter below 5μm. However, from a numerical point of view the number of small flakes is bigger than the number of large flakes.

In order to systematically represent this tendency we conducted size distribution statistics. Several standard samples were prepared in the same condition and imaged by SEM randomly from one edge of substrate to the other side. We have counted and studied approximately 2000 flakes, which are organized as the number of flakes and the ratio to total area of all flakes depending on each area, as shown in Figure 19.

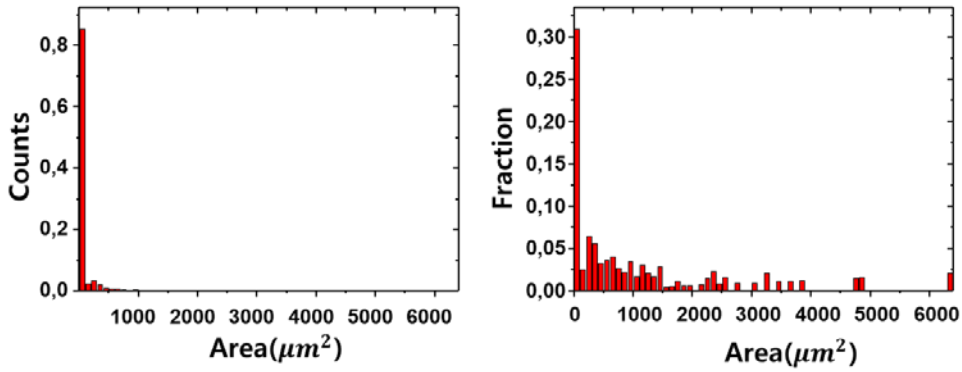

Figure 19 Area distributions of all GO flakes according to (a) the number of GO flakes for a certain flake area, (b) the relative size contribution with respect to the total area.

The range of GO flakes size is quite wide. The minimum is only below 1μm^2, while the maximum is around 5000 μm^2. In this graph, the highest contribution is the smallest part, corresponding to flake areas below 100 μm^2. Then the question arises: how a flake of 100 μm^2 can be considered "small or big"? In fact, there is no absolute criterion in the size of GO flakes. The criteria for classification of these middle size flakes can be considered quite arbitrary since even if we can obviously recognize extreme large or small size from a qualitative point of view, there is nothing precise about the numerical value. For example, 100 μm^2 belongs to smallest region in our data, whereas it is considered as large flakes in the literature. [31]

In reference to a recently published article,[31] ~ 3.5 μm^2, ~50 μm^2, ~240 μm^2 ~1000 μm^2 are classified as small, large, very large, ultra large flakes, respectively. Following this classification, namely Weibull model, 77% of GO we synthesized are large flakes and half of that is ultra large flakes. Therefore we can say that our GO flakes mainly consist of large flakes. The classification of the size distribution following this model is shown in Figure20.

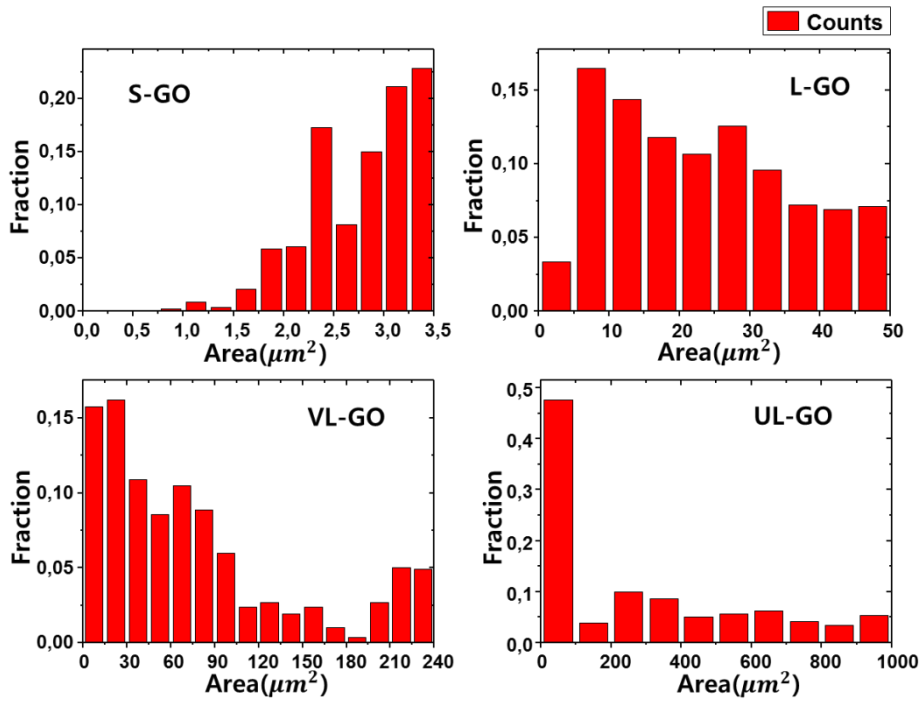

Figure 20 Area distributions of GO flakes divided in different size groups following the classification proposed in reference[31] ; S-GO, L-GO, VL-GO, UL-GO.

6.3.2 Lyotropic LC phase of GO

Large size GO sheets with high aspect ratio have a lot of advantages compared to small flakes for device applications, because defect ratio in large flakes is less than that of small flakes. Furthermore, large GO flakes in water, as a colloid state, can form nematic liquid crystalline (LC) phases due to high aspect ratio. The simple scheme of LC formation by GO is shown in Figure 21C. Each GO flake has its orientation, indicated with the red arrow perpendicular to the flake surface, but on average they assume a common orientation, indicated by the director **n**.

Although our GO flakes contain a high quantity of large flakes there are also small flakes. It would be desirable to be able to select only certain sizes thus narrowing

the size distribution of flakes in suspension. In particular it would be interesting to have mainly only large flakes. We plan to make a size sorting of GO using their ability to form nematic liquid crystalline phases, [32] similarly as done with carbon nanotubes. [33] First, for this separation, we should know the threshold concentration between LC and isotropic phases. We observed that if a GO solution is below the concentration for which a full LC phase can be observed, this solution will spontaneously or very easily (after light centrifugation) separate into two phases: a clear isotropic solution on top and a liquid crystalline phase below. This behavior is not surprising because it is expected a region of coexistence of isotropic and liquid crystal phase. LC phase part might consist of large flakes due to the property that larger flakes of GO can form LC phases more easily than smaller ones. Therefore it is important to understand the LC behavior estimating when the phase transitions occur and its behavior.

The LC phases were checked at different concentration of GO to determine the threshold concentration. We prepared several series of GO suspension at different concentrations as shown in Figure21A. Then they were observed between macroscopic crossed polarizers as shown in Figure21B to detect the appearance of birefringence. The suspensions were also filled into capillaries and checked in an optical microscope between crossed polarizers, see Figure21D displaying the birefringence texture of 1mg/ml GO suspension. We observed the formation of the typical texture until a concentration of 0.05g/ml of GO as threshold concentration.

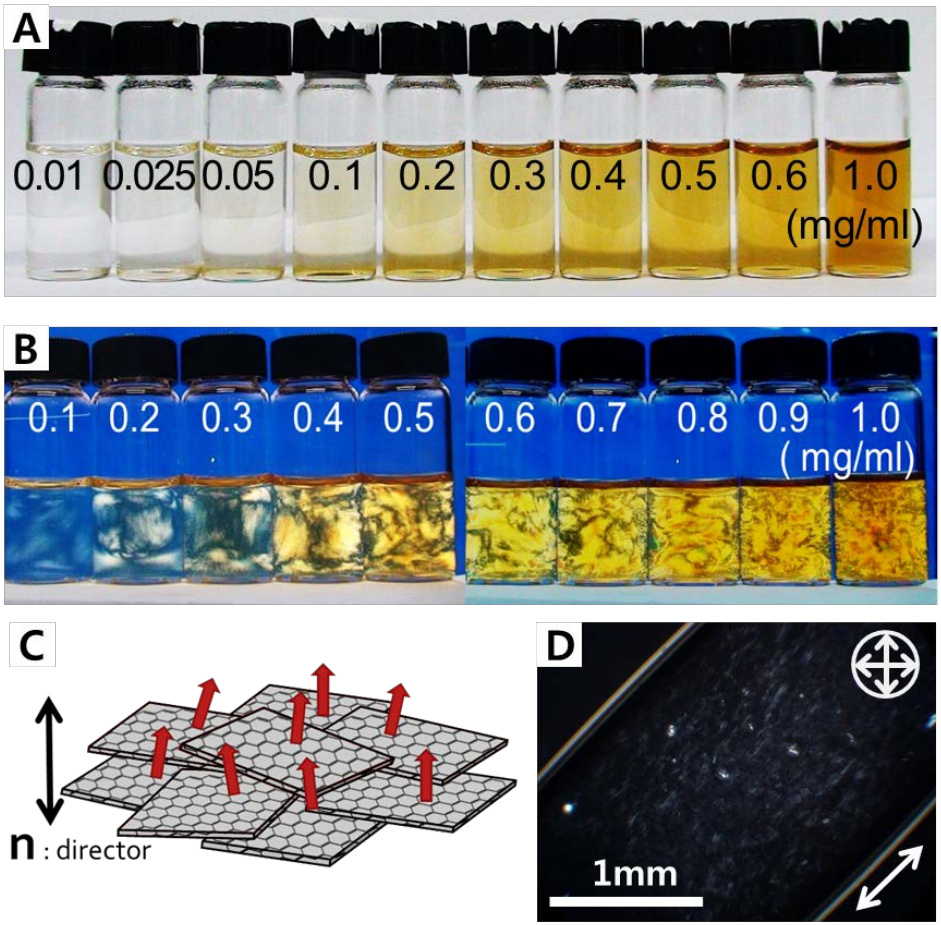

Figure 21 (A) The series of GO suspension at different concentrations (B) between macroscopic crossed polarizers. (C) The simple scheme of LC formation by GO. The average alignment direction of GO flakes was indicated as n. (D) The birefringence texture of 1 mg/ml GO suspension filled into a capillary.

6.3.3 Graphene/Chromophore system for photovoltaic cell

Exciton produced by photon of light is separated as hole and electron which diffuse into opposite directions. Then, currents flow by movement of hole and electron between anode and cathode. To realize solar cell it is one of the crucial points that separated charges efficiently flow to the electrodes where intimately fabricated matrix of donor and acceptor is a way to enable achievement of high efficiency. [34,

[35] Here we chose graphene/graphene oxide as electron acceptor and porphyrin as electron donor, [36] where the key concept is liquid crystalline assembly [37] for enhanced photocurrent.

In general graphene oxide possesses negative charges due to the presence of oxygen atoms on the carbon framework., Negatively charged porphyrin which possesses four $SO_3^-Na^+$ functional groups ($SO_3^-Na^+$-porphyrin is hereafter referred to as porphyrin) was chosen to bind with GO. Positively charged porphyrins provoke the formation of aggregates due to strong electrostatic interactions between the graphene flakes and the porphyrin. We have also tested neutral porphyrin; unfortunately, it is not enough soluble in water to be mixed with GO. Negatively charged porphyrins were well soluble in water without any aggregation or sediment and made a homogeneous suspension with GO. We prepared samples with the ratio between GO and porphyrin equal to 250:1. In Figure 22A, left vial is GO suspension which consists of only GO as reference and right vial is GO/porphyrin mixture sample. Although they contain the same concentration of GO, the right vial is darker than the left one because of porphyrin color. We observed birefringence to check if liquid crystal phases of GO suspension still existed or not after adding the porphyrin. As shown in Figure 22B, birefringence was observed between macroscopic crossed polarizers as demonstrating that the long-range organization is conserved.

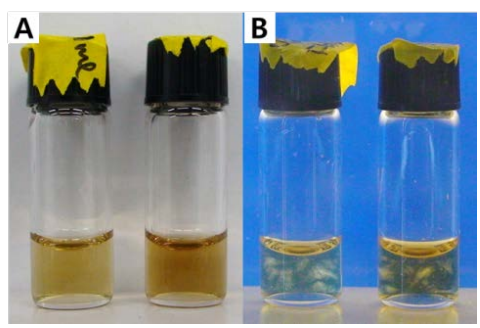

Figure 22 (A) GO suspension (left) and GO/porphyrin mixture (right) (B) observed

by cross-polarized optical microscope. The two vials contain the same quantity of GO.

Even if weaker than in the pure sample, a fluorescence signal still appeared in the GO/porphyrin mixture and this feature has been used to observe the distribution of the chromophore in the GO LC phases by confocal microscopy. Sample of GO/porphyrin were observed by fluorescence and polarized optical microscopy after being filled into flat capillaries. Different ratios between GO and porphyrin, 25:1, 6.25:1, 2.5:1, 0.25:1 were prepared and investigated. The images of Figure 23 indicate the distribution of the porphyrin within the GO host through the detection of its fluorescence. The fluorescence signal was uniform throughout the capillary except the parts near the edges of capillary. The possibility of the less fluorescence signal can be due to effect of edge wall in capillary. This shows that the porphyrin is well distributed in the liquid-crystalline phase and that there is no phase segregation. When we increased the amount of porphyrin, the fluorescence signal became stronger and saturated for the ratio equal to 0.25:1.

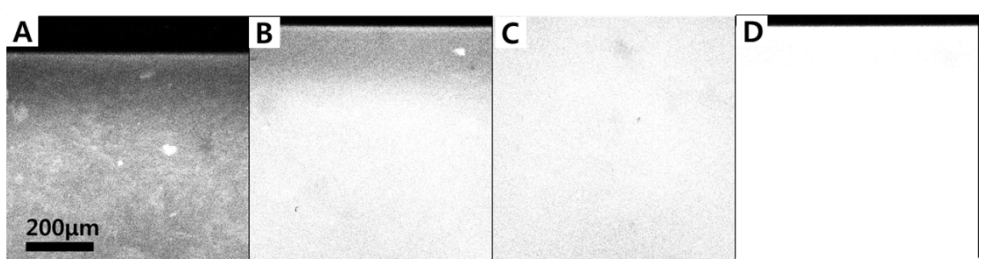

Figure 23 Fluorescence microscope images obtained for GO/porphyrin mixtures as different ratio (A) 25:1, (B) 6.25:1, (C) 2.5:1, (D) 0.25:1.

After mixing graphene oxide with porphyrin and verifying the liquid crystalline properties of the resulting materials, we performed the reduction of the graphene oxide. Graphene oxide is a completely insulating material and in order to get charge flow to the electrodes, it has to be reduced. Several methods have been

reported in literature, [30] as described in section 6.2.3 our reduction process was based on the thermal heating of graphene oxide at 150°C under reductive atmosphere. After reduction procedure, we observed that the brown materials turned black which means a reduction of the graphene oxide and the formation of reduced graphene oxide (rGO).

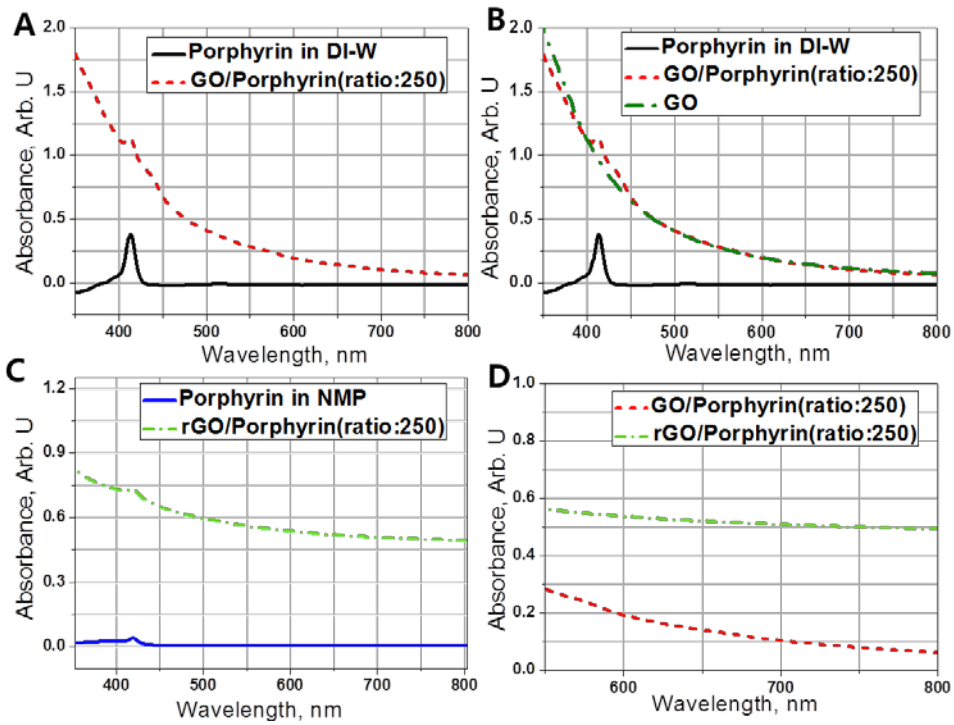

Figure 24 The optical spectra of (A) porphyrin and GO/porphyrin mixture (the ratio between GO and porphyrin is equal to 250:1) (B) with GO suspension with same concentration as GO/porphyrin and (C) porphyrin and rGO/porphyrin mixture with 250:1 ratio, (D) in comparison with GO/porphyrin and rGO/porphyrin.

Optical absorption measurements of GO/porphyrin and rGO/porphyrin were carried out as shown in Figure 24. In Figure 24A, when only porphyrin is measured as reference, the main peaks appeared at 413nm. On the other hands, in the absorption spectra of GO/porphyrin, besides the main peak (413nm) a new peak appears shifted to the right by approximately 20nm, at 433nm. The intensity of

main peak seems to decrease compared to pure porphyrin in Figure 24B, where green line indicates only GO suspension with same concentration as GO/porphyrin. This, together with the appearance of the new peak suggests that there is a notable interaction between GO and chromophore.

The absorption spectra of porphyrin and rGO/porphyrin are shown in Figure 24C. First, both graphs of Figure24C the absorption peaks of the porphyrin were shifted to 420nm while that was at 413 nm in Figure 24A. These shifts can be due to aggregation of the chromophores in the organic solvent - NMP, or due to solvent effects, since there was not shift observed in Figure 24A. Second, the absorption peaks of the porphyrin and rGO/porphyrin in NMP are around found at 420 nm. It seems therefore that the porphyrin are better solvated in NMP and have less interactions with rGO. In Figure 24D, the absorption of light by rGO was higher than the absorption by GO although concentration of rGO in rGO/porphyrin is much lower than GO in GO/porphryin (When you compare porphyrin intensities, solid line in Figure 24A is much higher that solid line in Figure 24C. It is reasonable since they are same ratio.)

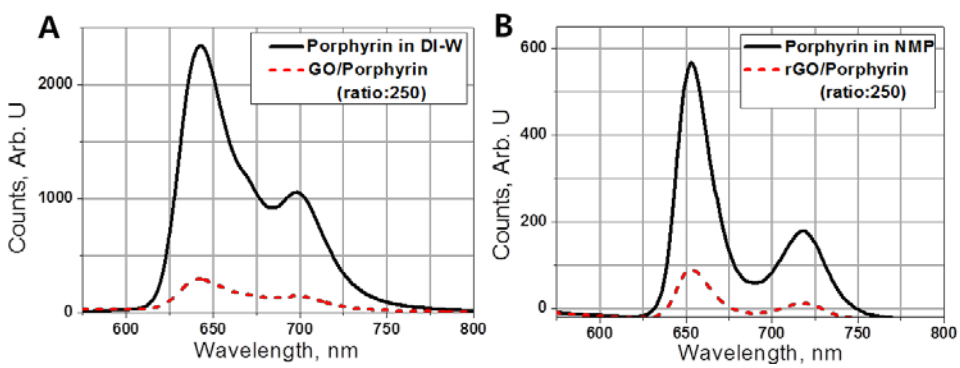

Figure 25 Fluorescence spectra of (A) porphyrin and GO/porphyrin mixture (the ratio between GO and porphyrin is equal to 250:1) and (B) porphyrin and rGO/porphyrin mixture with 250:1 ratio.

Measurements of the fluorescence signal were performed to check if there is any

emission transferred to (r)GO from the porphyrin, using the same reference and (r)GO/porphyrin mixture as we used for absorbance. The fluorescence spectra were shown in Figure 25A and 25B indicating GO/porphyrin and rGO/porphyrin, respectively. When the porphyrin was excited with a wavelength = 420 nm, two fluorescence peaks were observed at 643 and 703 nm in Figure 25A, at 653 and 719 nm in Figure 25B. These shifts seemed to be same reason with absorbance data (Figure 24). We observed that the GO/porphyrin and rGO/porphyrin had much lower amount of emission in comparison with each reference sample which consists of only porphyrin. At same time, quenched efficiency of the emission is higher in GO/porphyrin than in rGO/porphyrin hybrids. This shows that the porphyrin interacts with GO as proved that GO quenches the emission of porphyrin and porphryin is more efficiency quenched in GO environment comparing to rGO; there is energy or charge transfer between the porphyrin and the graphene oxide.

The most interesting results are the presence of interaction between porphyrin and GO/rGO and also the possibility to incorporate uniformly porphyrin in the LC GO preserving the long range order. It is also interesting that there is a difference of quenching efficiency between GO and rGO. From Figures 25, it is clear that GO quench more efficiently the fluorescence of the porphyrin than rGO; this is in accordance with the difference of absorption spectra between GO/porphyrin and rGO/porphyrin. Indeed for GO/porphyrin in water, a part of the porphyrin absorption is shifted a about 20 nm compared to porphyrin alone (413 vs 433 nm). This indicated a better interaction between porphyrin and GO in water than between porphyrin and rGO in NMP.

Two mechanisms can explain the quenching of the porphyrin fluorescence: photo induced energy or charge transfer. Because of the existing literature on the GO, [38] rGO/chromophores hybrids, [39, 40] we strongly believe that charge transfer occurs from the porphyrin to the GO/rGO. However, in order to help identifying the

mechanism, additional experiments are needed. For example, time resolved absorption spectroscopy could permit to identify the different porphyrin species in solution after light excitation and in particular oxidized porphyrin[41] that would prove photo induced electron transfer from the porphyrin to graphene.

References

[1] Qingbin Zheng et al., ACS Nano, **2011**, Vol. 5, No. 7, 6039-6051

[2] Da Chen et al., Energy Environ. Sci., **2013**, 6, 1362-1387

[3] Hideo Shimoda et al., Adv. Mater., **2002**, 14, No. 12

[4] B.W. Walters et al, Applied Physics Letters, **2000**, Vol. 77, No. 5

[5] Luca Valentini et al., Macromol. Mater. Eng., **2008**, 293, 867-871

[6] Yue Hu et al., Small, **2013**, 9, No. 8, 1306-1311

[7] Weiss et al., Langmuir **2006**, 22, 854-856

[8] E. Nativ-Roth et al., Small, **2008**, 4, 1459

[9] J. M. Bonard et al., Adv. Mater., **1997**, 9, 827

[10] Sarah Dolle et al. Angewante, **2012**, 51(13), 3254-3257

[11] J. Lagerwall et al., Adv. Mater., **2007**, 19, 359–364

[12] Giusy Scaliaet al., Phys. Stat. Sol. (b) **2007**, 244, No. 11, 4212-4217

[13] Giusy Scalia, ChemPhysChem, **2010**, 11, 333-340

[14] J. Lagerwall et al., phys. Stat. Sol. (b), **2006**, 243, 3046-3049

[15] G. Scalia et al., Soft Matter, **2008**, 4, 570-576

[16] Sumio Iijima, Nature, **1991**, 354, 56-58

[17] M. Reibold et al., Nature, **2006**, 444, 286

[18] Carbon Nanotube Reinforced comopsites: Metal and Ceramic Matrices. Sie Chin Tjong Copyright, **2009**, WILEY-VCH Verlag CMbH&Co. KGaA, Weinheim, ISBN:978-3-527-40897-4

[19] C. Lee et al., Science, 2008, 321, 385

[20] Bolotin, K. I. et al., Solid State Commun., 2008, 146, 351–355

[21] Balandin, A. A. et al., Nano Lett., 2008, 8, 902–907

[22] K. Hiltrop, Lyotropic Liquid Crystals in “Liquid Crystals”Stegemeyer H (guest ed.), Steinkopff Darmstadt, Springer New York, **1994**, 143-171

[23] J. Azevedo et al., J. Phys. Chem. C, **2011**, 115, 14678-14681

[24] Kathleen L. Herrington et al., J. Phys. Chem. **1993**, 97, 13892-13802

[25] A. Renoncourt, Study of supra-aggregates in catanionic surfactant systems, **2005**, Ph.D. thesis, Uni. Regensburg, Germany

[26] Mildred S. Dresselhaus et al., Nano letters, **2010**, 10(3), pp751-758

[27] G. S. Duesberg et al., Physical Review Letters, **2000**,85, 25, 5436-5439

[28] W. S. Hummers Jr et al., J. Am. Chem. Soc., **1958**, 80, 1339

[29] Daniel R. Dreyer et al., Chem. Soc. Rev., **2010**, 39, 228-240

[30] S. Mao et al.,RSC Adv., **2012**, 2, 2643-2662

[31] X. Y. Lin et al., ACS Nano, **2012**, 6, 10708-10719

[32] Zhen Xu et al., ACS Nano, **2011**, Vol. 5, No. 4, 2908-2915

[33] Wenhui Song et al., Science, **2003**, Vol. 302, no. 5649, 1363

[34] S. Günes et al., Sariciftci, Chem. Rev., **2007**, 107, 1324

[35] C. J. Brabec et al., Adv. Mater., **2010**, 22, 3839

[36] Hironobu Hayashi et al., J. Am. Chem. Soc., **2011**, 133, 7684-7687

[37] L. Schmidt-Mende et al., Science, **2001**, 293, 1119.

[38] Emanuele Treossi et al., J. Am. Chem. Soc., **2009**, 131, 15579-15577

[39] Aleksandra Wojcik et al., ACS Nano, **2010**, 4(11), 6697-6706

[40] Ian V. Lightcap et al., J. Am. Chem. Soc. **2012**, 134(16), 7109-7116

[41] H. Imahori et al., J. Am. Chem. Soc., **1996**, 118, 11771

요약 (국문초록)

탄소나노튜브(CNTs)와 그래핀은 유연하고 투명한 소자와 같은 미래산업이 요구하는 조건을 충족시킬 수 있어 매우 관심을 끄는 물질임에도 불구하고, 실제 산업의 응용에 있어서는 몇 가지 이유들로 인해 완벽한 가능성을 보여주기에 어려움을 겪고 있다. 탄소나노튜브는 튜브 사이의 반데르발스 힘에 의하여 응집이 일어나고, 이는 percolation 한계치의 증가와 성능의 저하를 불러일으키기 때문에 개별적으로 튜브를 분산해야 하는 문제를 지니고 있다. 게다가 탄소나노튜브의 물질적 특성은 강하게 비등방성이고, 획일적이고 조절 가능한 배열은 나노 유효범위의 특성을 거시적인 규모로 성능향상을 이끌어내는데 유용하다. 탄소나노튜브와 같이 그래핀 조각들 또한 그들의 비등방성 모양으로 인하여 좋은 배열을 조직하는데 장점을 가지고 있다. 그러므로 본 학위 논문에서는 자기 조직화된 탄소물질들을 두 가지 관점으로 설명하며 연구결과를 소개할 것이다: 1) 매우 낮은 농도의 계면활성제를 기반으로한 lyotropic 액정 시스템을 이용하여 탄소나노튜브의 분산과 배열, 2) 조직화된 산화그래핀의 광활성 합성물.

먼저, 계면활성제가 micelle을 형성하는 최소 온도를 뜻하는 Krafft 온도의 개념을 소개한다. 계면활성제는 탄소나노튜브의 분산에 유용하지만 초과된 여분의 양은 탄소나노튜브의 물질적인 특성을 저하시키고 또한 micelle을 형성하여 감손인력으로 인한 탄소나노튜브의 재응집을 일으킨다. Krafft 온도의 사용은 질적으로 좋은 분산액을 가져옴과 동시에, 탄소나노튜브 용액 내에서 계면활성제 양을

최소화하는데 있어 이점을 가지고 있다는 것에 대하여 이미 증명 되었다. 지금까지 그 과정은 상온 이하에서 불편하게 수행되었으나, 본 연구에서는 상온에서 편리하게 사용될 수 있는 OTAB (octadecyltrimethylammonium bromide) 계면활성제를 이용한 새로운 sub-Krafft 절차법을 소개한다. 탄소나노튜브의 분산과 계면활성제의 질적인 측정을 위하여 광학현미경과 광학분광법, 원자간력현미경(AFM)과 함께 수행되었다. Krafft온도 이상, 이하의 온도에서 분산된 시료를 비교한 결과 새로운 sub-Krafft으로 실험한 접근법이 우수한 성능을 보이는 것으로 분석되었다.
광학현미경에서 응집이 관찰되지 않았을 뿐만 아니라 더 높은 평균 흡수값과 강한 peaks이 광학분광법에 의해 측정되었다. 더 좋은 질적인 분산은 AFM을 통해 나노 스케일에서 확인 되었다.

계면활성제를 기반으로한 lyotropic 액정은 효과적은 탄소나노튜브의 정렬을 위한host 물질로 사용된다. 감소된 계면활성제 양으로 lyotropic 액정을 형성하기 위하여 본 연구에서 수행한 핵심적인 방안은 양이온과 음이온 계면활성제의 조합을 사용하는 것이다. sodium dodecyl sulphate (SDS) 와 dodecyltrimethylammonium bromide (12TAB) 두 계면활성제의 몰비율을 조절하여 편광현미경으로 액정상의 형성을 관찰하면서 그 효과를 조사하였다. 그 결과, 전형적인 lyotropic 액정상이 20wt% 이상에서 획득되는 것과 비교하면 매우 낮은 양인 8wt%에서 액정상을 구현하는 데 성공하였다. 액정 host에 탄소나노튜브가 포함되어 조합되었고 광학현미경과 편광현미경에 의해 관찰 되었다. 액정-탄소나노튜브 복합체로부터 형성된 실과 같은 형태의 섬유질 내에서 탄소나노튜브의 정렬이 편광 라만분광법에 의해

관찰 되었다.

화학적 방법에 의한 그래핀 합성에서 중간 단계 형성물인 산화그래핀은 수용액 상태의 특정 농도 이상에서 nematic 액정상을 보일 수 있다. 이것은 산화그래핀 수용액이 lyotropic 액정 시스템이라는 것을 의미한다. 본 연구에서는 매우 큰 조각들을 가지는 산화 그래핀의 액정상의 광학적 특성을 여러 농도에서 보여준다. 발색단의 종류 중 하나인 포르피린 유도체와 산화그래핀이 결합한 시스템의 액정 특성 또한 조사되었다. 액정상에 의하여 발색단을 포함한 그래핀의 방향 질서는 광전지와 같은 응용에 있어서 매우 흥미로운 시스템이다. 산화그래핀/포르피린, 환원된 산화그래핀과/포르피린 혼합물은 광학스펙트럼과 형광분석법에 의한 quenching 현상으로부터 확실한 상호작용을 보여주었다.

주요어 : 탄소나노튜브, 액정, 산화 그래핀, 자가조립, 나노 복합체, 광전지

학 번 : 2012-22453